NTNU
Norwegian University of
Science and Technology

Numerical simulation of a droplet-film collision using a phase-field approach

Erik Os Tengs

NTNU

Norwegian University
of Science and Technology

Department of Energy
and Process Engineering

MASTER THESIS

for

Student
Erik Os Tengs

Spring 2016

Numerical simulation of droplet-film collision using a phase field approach

Numerisk simulering av dråpe-film kollisjon med en phase-field metode

Background and objective

Computational fluid dynamic (CFD) represents a valuable and modern tool for performing computational experiments. CFD can be used in conjunction with experiments in order to gain better understanding of the physics involved in a given flow situation. A Navier-Stokes numerical solver based on a spectral element framework is available in the group. The solver is coupled to a phase field model in order to describe interface dynamics by using a diffuse interface approach. The phase field model is based on the minimization of the free energy of the system. As such, it does not need any a-hoc rule for the coalescence of interfaces.

The project will focus on the simulation of droplet-film coalescence. The results will be used to evaluate the performance of the code which has never been tested for such cases. The effect of fluid and flow parameters on the simulation outcome will be studied. In particular, the ability of the model to predict the bounding regime will be investigated.

The following tasks are to be considered:

1. Literature review on droplet-film coalescence, for the case of thick liquid films.
2. Setup of a reference simulation case for the simulation of the phenomenon, with proper boundary conditions.
3. Effect of spatial resolution and fluid and flow parameters on coalescence outcome.

Within 14 days of receiving the written text on the master thesis, the candidate shall submit a research plan for his project to the department.

When the thesis is evaluated, emphasis is put on processing of the results, and that they are presented in tabular and/or graphic form in a clear manner, and that they are analyzed carefully.

The thesis should be formulated as a research report with summary both in English and Norwegian, conclusion, literature references, table of contents etc. During the preparation of the text, the candidate should make an effort to produce a well-structured and easily readable report. In order to ease the evaluation of the thesis, it is important that the cross-references are correct. In the making of the report, strong emphasis should be placed on both a thorough discussion of the results and an orderly presentation.

The candidate is requested to initiate and keep close contact with his/her academic supervisor(s) throughout the working period. The candidate must follow the rules and regulations of NTNU as well as passive directions given by the Department of Energy and Process Engineering.

Risk assessment of the candidate's work shall be carried out according to the department's procedures. The risk assessment must be documented and included as part of the final report. Events related to the candidate's work adversely affecting the health, safety or security, must be documented and included as part of the final report. If the documentation on risk assessment represents a large number of pages, the full version is to be submitted electronically to the supervisor and an excerpt is included in the report.

Pursuant to "Regulations concerning the supplementary provisions to the technology study program/Master of Science" at NTNU §20, the Department reserves the permission to utilize all the results and data for teaching and research purposes as well as in future publications.

The final report is to be submitted digitally in DAIM. An executive summary of the thesis including title, student's name, supervisor's name, year, department name, and NTNU's logo and name, shall be submitted to the department as a separate pdf file. Based on an agreement with the supervisor, the final report and other material and documents may be given to the supervisor in digital format.

☐ Work to be done in lab (Water power lab, Fluids engineering lab, Thermal engineering lab)
☐ Field work

Department of Energy and Process Engineering, 13. January 2016

Olav Bolland
Department Head
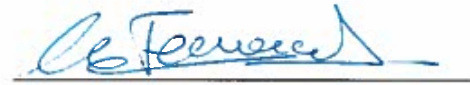
Maria Fernandino
Academic Supervisor

Research Advisor:

Preface

The thesis "Numerical simulation of a droplet-film collision using a phase-field approach" is the final piece of my Master's degree in Mechanical Engineering at the Norwegian University of Science and Technology (NTNU). I have been working on the thesis from January to June 2016.

The thesis is part of a research project at the "Thermal Two-Phase Flow Laboratory" at NTNU, where a brand new solver for multiphase flow is developed. My role in the project has been to test the solver performance and hopefully provide input as to what needs to be done in the future.

The intended readers of the following thesis are other Master's students, primarily within Flow engineering or similar. Parts of the mathematics and physics encountered later is graduate level, however all derivations do not need to be understood for the rest of the thesis to make sense. A set of videos are attached as a visual aid for when reviewing the results of the thesis.

Trondheim, 2016-06-09

Erik Tengs

Acknowledgments

I would like to thank the following persons for their great help during my Master's thesis:

My supervisor, Professor Maria Fernandino, who have been extremely helpful and supporting, and who I would like to thank for the opportunity I was given in writing this thesis.

Keunsoo Park, PhD-student at NTNU, whose solver I have used in the simulations. He has been of great help in dealing with the technical problems that inevitably arose.

Finally, I would like to thank all the fellow students, faculty and friends at the "Hydropower Lab" at NTNU, who all have made this final year great.

E.T.

Summary

Computational Fluid Dynamics is the science of solving the governing equations of fluid motion numerically. Simulating multiphase flow has traditionally been difficult, due to non-uniform fluid properties and challenges in expressing the interfacial forces. A solver developed by the "Thermal Two-Phase Flow Laboratory" at the Norwegian University of Science and Technology, has implemented a phase-field approach in order to model the interface dynamics of multiphase flow. The goal of this thesis is to simulate low energy droplet-film collisions using this solver, and test its performance.

Central to the phase-field approach is the Cahn–Hilliard equation. The equation model phase separation, and in simulations without convection, the solver was proven to be very successful. One and two droplets were simulated with ease. Several guidelines have been developed regarding what numerical resolution is needed to obtain good solutions.

In simulations where the coupled Navier–Stokes and Cahn–Hilliard equations were used to model droplet-film collisions, several errors were uncovered. Most notably was the global mass loss observed for some given problem setups. The solver was also seen to be highly parameter dependent, without discovering the definite underlying solution. Even though mass was not conserved globally, many promising signs were observed with respect to the dynamical behaviour of the collisions. Coalescence, one of the known possible collision outcomes, was obtained, as well as early signs of a bouncing droplet.

A proper mesh refinement and parameter study is recommended as further work in order to correct the errors discovered. Some of the physical behaviour is highly encouraging, and if the issue of mass conservation is corrected, the solver is believed to be a great tool in future multiphase simulations.

Sammendrag

Computational Fluid Dynamics er vitenskapen som omfatter numerisk løsning av de universelle likningene for fluiders bevegelse. Flerfasestrømning har tradisjonelt vært vanskelig å simulere, på grunn av ikke-uniforme fluid-egenskaper og problemer med beskrivelsen av kreftene i overflaten mellom fluider. En løser utviklet av " Thermal Two-Phase Flow Laboratory" ved Norges teknisk-naturvitenskapelige universitet, har implementert en "phase-field approach" for å modellere overflatedynamikken i flerfasestrømning. Målet i denne avhandlingen er å simulere en lav-energi kollisjon mellom en dråpe og en fluidfilm ved å bruke denne løseren.

Sentralt i "the phase-field approach" er Cahn–Hilliard likningen. Likningen modellerer faseseparasjon, og i simuleringer uten konveksjon, viser løseren seg å fungere veldig bra. Både én og to dråper ble simulert uten problemer. En rekke retningslinjer for nødvendig numerisk oppløsning er utviklet.

I simuleringer der de koblede Navier–Stokes og Cahn–Hilliard likningene ble brukt til å modellere dråpe-film kollisjoner, ble det funnet en rekke feil. Viktigst var et stort globalt massetap ved enkelte oppsett. Løseren var også svært parameter avhengig, en endelig løsning på problemet har ikke blitt funnet. Selv om løseren viste massetap, var flere av de dynamiske resultatene lovende. Koalesens, ett av flere mulige kollisjonsutfall, ble observert, samt antydninger til en dråpe som spretter på fluidfilmen.

En grundig raffinering av elementnettet og et parameterstudie er anbefalt videre arbeid for å forbedre feilene i løseren. Enkelte av de fysiske resultatene er lovende, og hvis problemet med massetap forsvinner, kan løseren bli et godt verktøy for løsning av flerfasestrømning.

Contents

List of Tables

List of Figures

Nomenclature

Frequently used Abbreviations		Units
Bo	Bond Number	[-]
CFD	Computational Fluid Dynamics	
CH	Cahn–Hilliard	
Ch_L	Cahn Number based on numerical cell	[-]
Ch_r	Cahn Number based on droplet radius	[-]
DI	Diffuse Interface	
L_i	Domain length in i-direction	[m][1]
LSQ	Least Squares Method	
Ne_i	Number of elements in i-direction	[-]
NS	Navier–Stokes	
Oh	Ohnesorge Number	[-]
P	Polynomial expansion	[-]
Re	Reynolds Number	[-]
SEM	Spectral Element Method	
We	Weber Number	[-]

---

[1]Physical units. Non-dimensional parameters have been used in the simulations.

Frequently used Symbols		**Units**
ϵ	Interface parameter	$[m]^2$
g	Gravitational Acceleration	$[m/s^2]$
λ_i	Ratio of parameter i	[-]
μ	Dynamic Viscosity	$[kg/(m \cdot s)]$
μ_0	Chemical Potential	$[kg/(m \cdot s^2)]$
r_0	Initial Droplet Radius	[m]
ρ	Density	$[kg/m^3]$
σ	Surface Tension	$[kg/s^2]$
Δt	Size of timestep	[s]
ϕ	Order Parameter	[-]
ψ	Bulk energy density	$[kg{\cdot}m/s^2]$
$\vec{u}$	Velocity Field	[m/s]

---

[2]Physical units. Non-dimensional parameters have been used in the simulations.

Chapter 1

Introduction

1.1 Background and Motivation

Fluid motion can be described by the Navier–Stokes (NS) equations. The NS equations are based on Newton's second law, $\vec{F} = m\vec{a}$, and are in essence a conservation of linear momentum. The NS equations are non-linear, second order, partial differential equations. Because of its complexity, it is only possible to analytically solve easy problems where several assumptions and simplifications have been made. This give rise to the branch of fluid mechanics called Computational Fluid Dynamics (CFD). In CFD, the goal is to solve the governing equations of fluid motion numerically. Solving multiphase flow however, has proven to be difficult due to non-uniform fluid properties and challenges in modelling interfacial forces.

Multiphase flow is defined as simultaneous flow of fluids with different properties. Examples range from steam droplets in boiling water, to water droplets in an oil pipe. The fluids can have a constant volume fraction, or undergo a phase-change, and thus vary with time (e.g. boiling water). Multiphase flow occurs in a number of applications. Power plants and process stations are examples where two-phase flow is present, and knowledge of heat transfer and pressure drop is crucial if one wants to design successful systems.

The interface between two fluids is of great interest, as it is where properties change values. In a CFD solver, the interface has to be modelled, and several models exist. Some models assume a sharp interface with instantaneously changing properties, other models, diffuse interface models (DI), assume the interface of having a finite thickness and continuous fluid

1

properties. The latter will be used in this thesis.

A droplet colliding with a fluid film is a fundamental phenomenon in multiphase flow. The problem is very complex, and while some references have successfully simulated high energy coalescence and bouncing droplets, none have been able to simulate low energy coalescence. This thesis will use a DI model called the phase-field method to model interfacial dynamics, that hopefully will change that. The advantage of using a phase-field approach is to avoid using an ad-hoc hypothesis regarding the coalescence of the two fluid bodies.

1.2 Goal and scope

The goal of this thesis is to numerically simulate the multiphase phenomenon of a droplet falling on a thick fluid-film of the same liquid. The simulations will be performed using a solver based on the spectral element method, and the phase-field approach will be used to model the interface dynamics. The Cahn–Hilliard equations will first be used to model phase separation, then coupled with the Navier–Stokes equations to solve dynamic problems. Figure 1.1 shows the different phenomena simulated in the thesis.
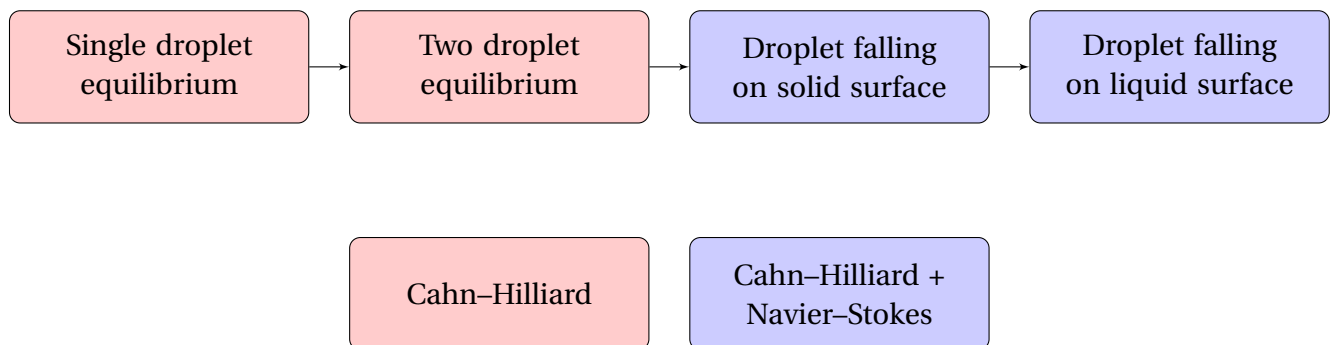
Figure 1.1: Overview of phenomena simulated in thesis

The scope of the thesis is as follows; two-dimensional, incompressible flow with no thermal effects will be considered. The density ratio of the fluids will be large, and the viscosity ratio will vary. The effect of the Weber number (We) at impact will be investigated, and in particular, bouncing/low energy coalescence is the desired outcome. Therefore, simulations will be limited to small We. The numerical implementation of the phase-field method will not be covered

in detail; an overview of the theory will be presented. General guidelines for how to set up a simulation, parameters, grid refinement and more, will be investigated and discussed.

A solver is provided to the author, and will be modified to simulate phenomena relevant to this thesis. The solver is developed at the "Thermal Two-Phase Flow Laboratory" at the Norwegian University of Science and Technology (NTNU). The simulations are performed in Matlab using the Vilje HPC-cluster available at NTNU. An MPI version of the solver will be used to perform the calculations efficiently and within a reasonable timeframe.

1.3 Structure

The thesis is set up as follows: Chapter 2 will cover the theory regarding the mathematical model, the numerical model and the dynamics involving falling and colliding droplets. A review of the experimental and numerical works in the field will also be presented. Chapter 3 will describe the different simulations performed. Chapter 4 will present the results from the simulations. Chapter 5 will discuss the results, investigate sources of error, and explain the assumptions made. Finally, chapter 6 will summarize the results and present recommended further work.

Appendix A list all the parameters and settings used in the simulations. If not explicitly stated otherwise, all simulations will follow the settings set there. Non-dimensional equations are used in the simulations, and thus, all parameters are dimensionless by definition. Figures will therefore not include units, although time frequently will be referred to as seconds. A sample Matlab code solving the Cahn–Hilliard equation is included in appendix B. Interested readers are encouraged to try the code and investigate the influence of the controlling parameters. Appendix C gives an introduction to numerical integration, and appendix D discusses the implementation of non-dimensional parameters. Finally, appendix E lists the videos attached with this thesis. It is highly recommended to watch the videos in conjunction with the result chapter, as they give a superior visual understanding of the dynamics.

Chapter 2

Theory

The purpose of this thesis is to numerically simulate a droplet-film collision. The interface dynamics in multiphase flow is usually complex, and developing a trustworthy model for the surface is of great interest. This thesis will use a solver where the phase-field approach is implemented in order to model the interface.

The first section in this chapter will cover the mathematical model; the Navier–Stokes equations and the phase-field approach. The next section will cover the numerical model, in particular, the spectral element method and the least squares method. The last section will cover the physical phenomena of droplet-film collisions, as well as a literary review of similar experiments and simulations.

2.1   The Equations of Fluid Motion

The goal to derive a set of equations that describes the motion of fluids. Fluids are substances that, unlike solids, deform under all external shear forces. Due to the low internal resistance in fluids, tracking one single particle is difficult, and it is common to adopt a Eulerian frame of reference. Several conservation laws can be derived, the ones relevant to this thesis are the conservation of mass, and conservation of momentum.

The equations for conservation of mass, usually referred to as the *continuity equation*, for incompressible flow, can be written as follows:

$$\nabla \cdot \vec{u} = 0 \tag{2.1}$$

where $\vec{u}$ is the velocity vector. The equations for conservation of momentum, usually referred to as the *Navier–Stokes equations* (NS), for incompressible flow, can be written as follows:

$$\frac{\partial \vec{u}}{\partial t} + \vec{u} \cdot \nabla \vec{u} = -\frac{1}{\rho} \nabla p + \frac{\mu}{\rho} \nabla^2 \vec{u} + \vec{g} \tag{2.2}$$

where $\rho, p, \mu, \vec{g}$ is the density, pressure, dynamic viscosity and gravitational acceleration respectively. We have assumed Newtonian flow with gravity as the only body force. The reader is expected to have some experience with the continuity and Navier–Stokes equations, a thorough derivation of the above equations can be found in many text books, e.g. Kundu and Cohen (2008).

2.2 Phase-Field Method

One of the problems with simulating multiphase flow is how to model the interface. Some approximations assumed that the surface was a layer of zero thickness, where physical properties are discontinuous across the surface. This is called the sharp interface model. Rayleigh (1892) then developed the idea that the surface has non-zero thickness, and van der Waals (1893) explained this by use of thermodynamical principles. This idea is called the diffuse interface model. Figure 2.1 shows the fundamental difference between the two models.
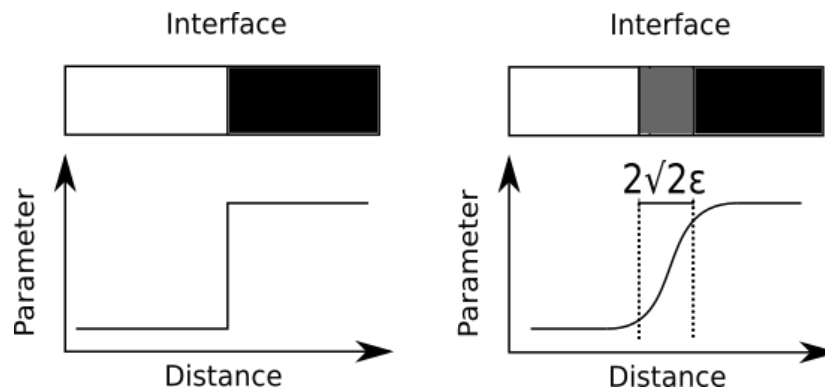
Figure 2.1: (a) Sharp Interface Model   (b) Diffuse Interface Model

In classical fluid mechanics, the sharp interface model is widely used, and it is largely suc-

cessful. There are however, situations where the model breaks down. This occurs when the thickness of the interface is comparable to the length scale of the problem at hand (Anderson et al. (1998)). In addition, sharp interface models cannot reproduce topological changes like coalescence and breakup, without the use of ad-hoc rules. A droplet falling on a film falls within this category, and the idea of a diffuse interface is therefore what will be adopted in this thesis. Another advantage with the diffuse interface model is that you avoid discontinuities and delta functions, thus making numerical simulations more suited.

The diffuse interface model used in this thesis is the phase-field method, a short derivation follows. Central to the method is the use of the free energy density, f. The free energy is a model for the energy in the system, composed of two parts, an interfacial energy and a bulk energy:

$$f = \frac{1}{2}\epsilon\sigma\alpha|\nabla\phi|^2 + \epsilon^{-1}\sigma\alpha\psi(\phi) \tag{2.3}$$

where the order parameter ϕ is a measure of phase, ϵ is a measure of interface thickness, σ is the surface tension coefficient, and $\psi(\phi)$ is the bulk energy density. The bulk energy density is described using a double-well potential, $\psi(\phi) = \frac{1}{4}\phi^2(1-\phi)^2$, a function with minima at $\phi = \{0, 1\}$, see figure 2.2a. The two minima are defining the value of ϕ in the two bulk phases.

(a) Bulk energy density ψ (b) General solution of order parameter ϕ
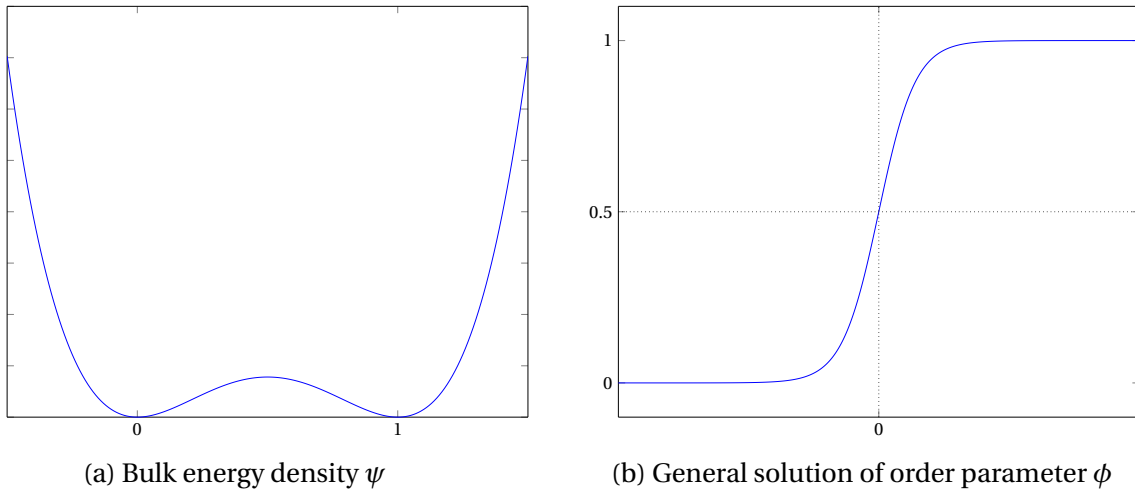
Figure 2.2: Free energy components

At equilibrium, the free energy $F = \int f dV$ is at a minimum,

$$\frac{dF}{d\phi} = \epsilon^{-1}\sigma\alpha\psi'(\phi) - \epsilon\sigma\alpha\Delta\phi = \mu_0 = 0 \tag{2.4}$$

where μ_0 is called the chemical potential. The one-dimensional solution to the equation $\mu_0 = 0$ yields $\phi(x) = 0.5 + 0.5\tanh(x/(2\sqrt{2}\epsilon))$ with x=0 being the location of the interface (ϕ=0.5), see figure 2.2b. That is, ϕ will take the value of $\{0,1\}$ in the two bulk phases, and $0 \leq \phi \leq 1$ in the finite interface region. Different definitions of the bulk energy $\psi(\phi)$ exists in literature, this may lead to other minima, however the hyperbolic tangent shape of the solution ϕ(x) is always the same.

The next step is to develop a method for calculating the phase parameter ϕ. Cahn and Hilliard (1958) extended van der Waals ideas of a diffuse interface by creating an equation describing the development of ϕ as a function of the chemical potential:

$$\frac{\partial \phi}{\partial t} = M\nabla^2 \mu_0 \tag{2.5}$$

Eq. (2.5) is the famous Cahn-Hilliard (CH) equation. The CH equation is based on Fick's law, where M is a diffusion parameter called mobility. The Cahn–Hilliard equation was originally used to model phase separation, but have later been applied to a variety of problems, among others, multiphase flow. Interested readers can refer to Lee et al. (2014) for a mathematical, physical and numerical derivation of the Cahn–Hilliard equations. A sample MATLAB CH code is included in appendix B. In order to couple the CH eq. with fluid flow, one has the convective Cahn-Hilliard equation, as listed below:

$$\frac{\partial \phi}{\partial t} + \vec{u} \cdot \nabla \phi = \nabla \cdot M\nabla \mu \tag{2.6}$$

Important properties of the equation will be presented later. The convective Cahn–Hilliard equation is coupled to the momentum and continuity equations through the velocity field, and similarly, the momentum equations get a forcing term expressed using the chemical potential and the phase parameter. The result is a system of equations solving for multiphase flow. The non-dimensional, incompressible continuity, Cahn–Hilliard and Navier–Stokes equations with phase-field surface forces are as follows:

$$\nabla \cdot \vec{u} = 0 \tag{2.7}$$

$$\sigma\alpha[\epsilon^{-1}(\phi^2 - 3\phi/2 - 0.5) + \epsilon\Delta]\phi + \mu_0 = 0 \tag{2.8}$$

$$\frac{\partial \phi}{\partial t} + \vec{u} \cdot \nabla \phi - \frac{1}{Pe} \nabla \cdot (M \nabla \mu) = 0 \tag{2.9}$$

$$\frac{\partial \vec{u}}{\partial t} + \vec{u} \cdot \nabla \vec{u} = -\nabla p + \frac{1}{Re} \nabla \cdot [(\nabla \vec{u} + \nabla \vec{u}^T)] + \vec{f} \tag{2.10}$$

where $\vec{f}$ is the interfacial and body forces. The interfacial force in the present simulation is expressed as $\vec{F}_{\text{int}} = \mu \nabla \phi / Bo$, and the gravitational forces as $\vec{F}_g = \rho g / Fr^2$. Eq. 2.8 comes from inserting the definition of the bulk energy density into eq. 2.4.

There are several important dimensionless numbers in the simulations. The Reynolds number, $Re = \rho_A L V / \mu_A$, the Bond number, $Bo = \rho_A g L^2 / \sigma$, the Froude number, $Fr = V / \sqrt{gL}$, and the Peclet number, $Pe = Lu / (M \mu_0)$. The density in the momentum equations is defined as follows: The local averaged density is $\bar{\rho} = \phi \rho_A + (1 - \phi) \rho_B$, then, using fluid A as a scale, a dimensionless density is $\rho = \bar{\rho} / \rho_A$. The viscosity is defined in a similar fashion. Note that the dimensionless density and viscosity follow the same shape as the order parameter, as is desired. The numerical implementation of the above system of equations will not be covered in this text, interested readers can refer to Ding et al. (2007) or Jacqmin (1999) for more information.

2.2.1 Mass and Energy in the Cahn–Hilliard Equation

Two important properties of the Cahn–Hilliard equation, mass conservation and energy minimization, will be derived in this section. As will be shown, mass loss may be observed locally in CH simulations, even though mass is conserved globally.

Starting with the Cahn-Hilliard equation:

$$\frac{\partial \phi}{\partial t} + \vec{u} \cdot \nabla \phi = M \Delta \mu \tag{2.11}$$

$$\mu_0 = \frac{\partial F}{\partial \phi} = \epsilon^{-1} \sigma \alpha \psi'(\phi) - \epsilon \sigma \alpha \Delta \phi \tag{2.12}$$

and boundary conditions:

$$BC1: \quad \vec{n} \cdot \vec{u}|_{\partial \Omega} = 0 \tag{2.13}$$

$$BC2: \quad \vec{n} \cdot \vec{\nabla} \mu_0|_{\partial \Omega} = 0 \tag{2.14}$$

where $\partial \Omega$ is the boundary of the computational domain. Integrate eq 2.11 over the domain Ω,

$$\int_\Omega \frac{\partial \phi}{\partial t} + \int_\Omega \vec{u} \cdot \nabla \phi = \int_\Omega M \Delta \mu_0 \tag{2.15}$$

$$\frac{d}{dt} \int_\Omega \phi d\Omega + \underbrace{\int_\Omega \phi (\nabla \cdot \vec{u}) d\Omega - \int_{\partial\Omega} \phi \vec{u} \cdot \vec{n} d\partial\Omega}_{\text{Divergence Theorem}} = \underbrace{M \int_{\partial\Omega} \nabla \mu_0 \cdot \vec{n} d\partial\Omega}_{\text{Divergence Theorem}} \tag{2.16}$$

$$\frac{d}{dt} \int_\Omega \phi d\Omega + \underbrace{\int_\Omega \phi (\nabla \cdot \vec{u}) d\Omega}_{\text{Continuity}}{}^{\nearrow 0} - \underbrace{\int_{\partial\Omega} \phi \vec{u} \cdot \vec{n} d\partial\Omega}_{BC1}{}^{\nearrow 0} = \underbrace{M \int_{\partial\Omega} \nabla \mu_0 \cdot \vec{n} d\partial\Omega}_{BC2}{}^{\nearrow 0} \tag{2.17}$$

$$\frac{d}{dt} \int_\Omega \phi d\Omega = 0 \tag{2.18}$$

The quantity ϕ is conserved. As the density follow ϕ, this equates to a global conservation of mass. How the mass is spread in the computational domain however, is not governed by this result. It is therefore possible to experience local mass loss in the droplet.

The energy of the system can be defined by the Ginzburg-Landau functional:

$$F = \int_\Omega f d\Omega = \int_\Omega \left[\alpha \epsilon \sigma \frac{1}{2} |\nabla \phi|^2 + \epsilon^{-1} \alpha \sigma \psi(\phi) \right] d\Omega \tag{2.19}$$

which is the integral of the free energy density over the domain. The time derivative of the energy is as follows:

$$\frac{d}{dt} F = \int_\Omega \mu_0 \frac{d\phi}{dt} = \int_\Omega \mu_0 (\nabla \cdot (M \nabla \mu_0) - \vec{u} \cdot \nabla \phi) = -M \int_\Omega |\nabla \mu_0|^2 d\Omega \leq 0 \tag{2.20}$$

Observe that the rate of change in the energy is negative. The dynamics of the problem will try to minimize the energy F. This is a very important feature of the CH equation, recall that the bulk energy had minima in the two bulk phases, hence the dynamics favour phase separation. That is exactly why the CH equation is coupled with the NS equations for solving multiphase flow.

Shrinking droplet

As mentioned earlier, the goal of this thesis is to numerically simulate a falling droplet. Imagine the hypothetical situation where a small disturbance in the velocity field causes the radius of

the droplet to shrink ($\delta r < 0$), and due to mass conservation, the value of the order parameter to increase ($\delta \phi > 0$), see figure 2.3. This shift in mass is allowable if the energy in the system is decreasing, as derived above. Yue et al. (2007) derives the theoretical shift in mass in such a situation, along with numerical verification and the derivation of a stable lower limit for the droplet radius.
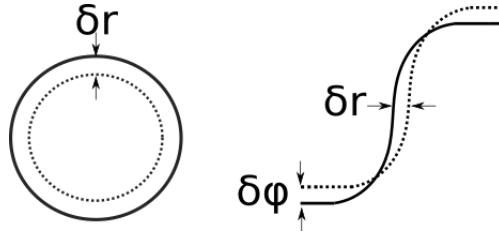
Figure 2.3: Shrinking droplet, top and side view

The result is repeated without further derivation:

$$\frac{\partial r}{r_0} = -\frac{\sqrt{2}}{24}(\frac{V}{V_d})(\frac{\epsilon}{r_0}) \tag{2.21}$$

$$\partial \phi = \frac{\sqrt{2}}{6}(\frac{\epsilon}{r_0}) \tag{2.22}$$

where V, V_d is the domain and droplet volume respectively. Observe that both change in droplet size and shift in phase parameter is governed by $(\frac{\epsilon}{r_0})$. $(\frac{\epsilon}{r_0})$ will later be referred to as a Cahn number Ch_r. A $Ch_r < 0.01$ gives negligible mass loss according to Yue et al. (2007). The above result can be used as a validation of the solver used in this thesis.

The volume ratio in the simulations should be low, however one has to be aware of the implications of the boundaries if the droplet is too large with respect to the domain. A lower limit for the droplet size with respect to the domain size can also be derived. If the droplet has an initial radius smaller than a critical radius, the droplet will disappear in a process similar to Ostwald ripening (Yue et al. (2007)). The critical radius is defined as follows:

$$r_c = \left(\frac{\sqrt{6}}{8\pi}V\epsilon\right)^{1/3} \tag{2.23}$$

The simulations in this thesis will be well within the limit above.

2.3   The Numerical Method

The Navier–Stokes equations are non-linear, second order, partial differential equations. The equations are usually impossible to solve analytically, unless several assumptions and simplifications have been made. This limits the direct use of the NS equations in engineering science. One highly successful approach in engineering is to construct non-dimensional versions of the equations, perform model experiments, before scaling to real size. This approach also has its limitations, as experiments can be difficult to perform, expensive and time-consuming. This illustrates the need for another approach to fluid mechanical problems. Computational Fluid Dynamics (CFD) is the science of solving the governing fluid mechanical equations numerically. The CFD community is growing and becoming more and more important as the price of computational power and memory is decreasing.

A numerical method needs several components. Firstly, there needs to be a mathematical model describing the physical phenomena. The models used in this thesis are described in section 2.1 and 2.2, culminating in the eqs. 2.7-2.10. Secondly a discretization method has to be chosen. This thesis will use the Least Squares Spectral Element Method, a brief introduction will follow. Finally, one has to choose an appropriate solution method, as the discretization produces a large system of non-linear algebraic equations. Figure 2.4 is showing the main parts of the numerical method.
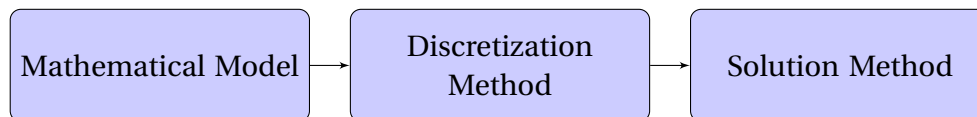
Figure 2.4: Ingredients in a numerical method

2.3.1   Spectral Element Method

The continuous differential equations from the mathematical model have to be approximated by a set of algebraic equations. There are several discretization schemes available, the most common are the finite difference method (FD), the finite volume method (FV) and the finite element method (FE). The FD method approximates the derivatives at one node by use of the function values at the neighbouring nodes. A node is a place in the domain where the differen-

tial equations are approximated. The FD method is easy to implement; however it is best used on structured grids. Conservation is not strictly enforced in FD methods. The FV method uses the integral form of the equations of motion. The conservation laws are applied to each CV, and the computational node is centered in the CV. FV methods can be used on all grid types, and conservation is guaranteed. The drawback is the complexity when implementing higher than second order schemes. The FE method approximates the solution within an element by a shape function, and ensures continuity (C^0 or better) across element borders. The element approximations are inserted into a weighted conservation law, then integrated over the entire domain. The FE methods are not strictly conservative, but have several advantages, among others the ability to handle arbitrary geometries and easy implementation of higher order schemes. An introduction to the FD and FV methods used in fluids mechanics can be found in Ferziger and Peric (2012), while a thorough description of the FE method can be found in Zienkiewicz et al. (1977), among others.

This section will briefly cover the basic concept of the Least Squares Spectral Element Method (LSQSEM). A thorough mathematical description is beyond the scope of this project, but can be found in other texts, see De Maerschalk (2003), Proot and Gerritsma (2002), Fernandino and Dorao (2011). The general concept of the Spectral Element Method is to divide the domain into elements, then write the solution within each element as a sum of weighted polynomials (2.24). The sum consists of a known basis function multiplied by a coefficient, and the assumption is that in the limit of this being an infinite sum, you would recover the exact solution. When writing the solution f^e on this form, and the basis functions $\phi_j(x)$ being known, the problem reduces to finding the coefficients α_j.

$$f^e(x) = \sum_{j=0}^{P} \alpha_j \phi_j(x) \tag{2.24}$$

Eq.(2.24) shows the mathematical description of the polynomial expansion, where P is the expansion order and ϕ_j is a basis function. The basis functions used in this solver are the orthogonal Hermite polynomials taken from Fernandino and Dorao (2011), see figure 2.5.

The Hermite polynomials consist of four basis functions that assign the value and first derivative at the boundaries. These functions are strictly necessary. Additional, optional "Bubble"

(a) Basis functions
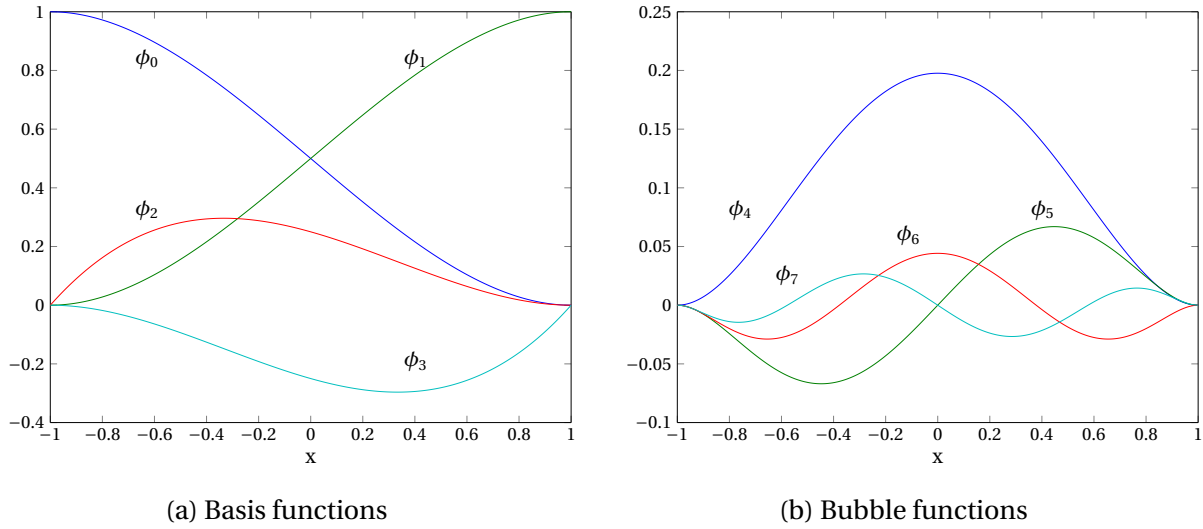
(b) Bubble functions

Figure 2.5: Hermite Polynomials

functions can be added to provide information about the inter-element values. Figure 2.5b shows four Bubble functions, however more functions can be made if needed. The higher polynomial order used, the more accurate results.

The solution in the whole domain is obtained by combining the solutions in each subdomain,

$$f(x) = \bigcup_{e=1}^{Ne} f^e(x) \tag{2.25}$$

with Ne being the number of elements.

The big advantage with using the Spectral Element Method is spectral or exponential convergence. In theory, if the solution is analytic or infinitely smooth, the convergence rate with respect to approximation order will be exponential. Exponential convergence is the fastest convergence possible, and it gives the method great error properties. If the function is not analytic, or in the case of discontinuities, this convergence rate will not be obtained, see Xiu (2010). Keeping a constant polynomial order P, and refining the mesh should display the same convergence rate as a method of order P, which for P>2 is superior to most commercial software.

In this thesis, the geometrical domain will be discretized into a uniform, structured, Cartesian grid.

2.3.2 Least Squares Method

The differential equations from arising from the mathematical model are discretized using the Least Squares Method. A general derivation follows:

Given the general differential equation,

$$\mathscr{L}f = g \qquad (2.26)$$

where $\mathscr{L}$ is a generic differential operator. Define the residual R:

$$R = \mathscr{L}f - g = 0 \qquad (2.27)$$

The residual will take the value of zero as the simulation approaches the exact solution f. If the residual is multiplied with a test function Φ and the integral over the new quantity is set to be zero, the result is a method for solving differential equations called the Mean Weighted Residual method (MWR):

$$\int_{\Omega} R\Phi d\Omega = 0 \qquad (2.28)$$

There are several possible choices of test functions. In the Galerkin method, the test functions are the same as the basis functions. In this solver, the residual itself is going to be used as the test function:

$$\int_{\Omega} R^2 d\Omega = 0 \qquad (2.29)$$

This method is called the Least Squares Method (LSQ). In reality, the residual of the numerical solution is not equal to zero. Define a functional J as half of (2.29). The goal is to minimize this quantity to find the best possible approximation of f,

$$J(f) = \frac{1}{2}\int_{\Omega} R^2 d\Omega = \frac{1}{2}\int_{\Omega} (\mathscr{L}f - g)^2 d\Omega$$

Now introduce the polynomial expansion from equation 2.24;

$$J(f) = \frac{1}{2}\int_{\Omega} (\mathscr{L}f - g)^2 d\Omega = \frac{1}{2}\int_{\Omega} \left(\sum(\alpha_j \mathscr{L}\phi_j) - g\right)^2 d\Omega = J(\alpha_0, \ldots, \alpha_N)$$

The functional J is only a function of the unknown coefficients α_j. To find the minimum of the functional J, set the partial derivative with respect to all coefficients to zero:

$$\frac{\partial J}{\partial \alpha_i} = 0, \qquad \forall i = 0 \dots N$$

$$\frac{\partial}{\partial \alpha_i}[\frac{1}{2}\int_{\Omega}(\sum(\alpha_j \mathscr{L}\phi_j) - g)^2 d\Omega] = \int_{\Omega}(\sum(\alpha_j \mathscr{L}\phi_j) - g)L\phi_i d\Omega = 0$$

$$\sum \alpha_j \int_{\Omega} \mathscr{L}\phi_j \mathscr{L}\phi_i d\Omega = \int_{\Omega} g\mathscr{L}\phi_i d\Omega \tag{2.30}$$

Eq. (2.30) can be expressed as a matrix system:

$$A_{ij}\alpha_j = F_i \tag{2.31}$$

with

$$A_{ij} = \int_{\Omega} \mathscr{L}\phi_j \mathscr{L}\phi_i d\Omega, \quad \alpha_j^T = [\alpha_0, \alpha_1, \dots, \alpha_M], \quad F_i = \int_{\Omega} g\mathscr{L}\phi_i d\Omega$$

where α_j^T is the unknown vector. The integrals above have to be dealt with numerically. In this thesis, Gauss quadrature integration will be implemented, more specifically, integration defined on the Gauss-Legendre-Lobatto (GLL) points. Interested readers can find an introduction in appendix C.

A big advantage of the least squares method is that it always transforms the partial differential equations to a symmetric positive-definite system, where effective solvers like the preconditioned conjugate gradient method can be used, see Bewley (2010) or Shewchuk (1994).

2.4 Dynamics of Droplet-Film collisions

Droplets colliding on liquid and solid surfaces are observed in many parts of the physical world, from spray-combustion and ink-jet printing, to meteorite impaction and multiphase flow. The controlling parameter in phenomena regarding droplet collisions is the Weber number (We) defined as follows:

$$We = \frac{2\rho_A V_0^2 R}{\sigma} \tag{2.32}$$

where ρ_A is the density of the heavy liquid, σ the surface tension, R is the radius of the falling droplet, and V_0 is the impact velocity, see figure 2.6. The Weber number is the ratio of the inertial forces to the surface tension forces.
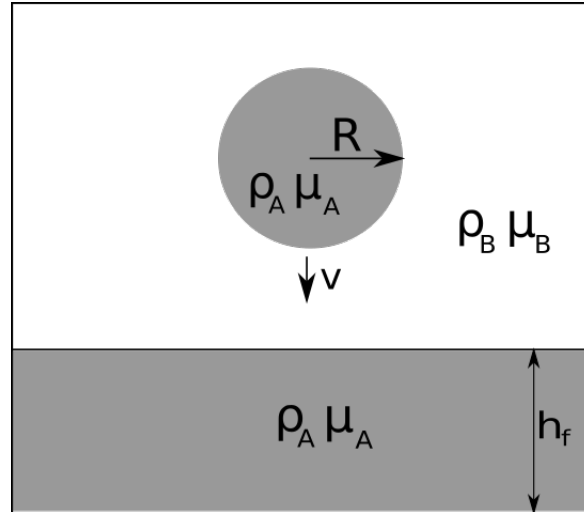
Figure 2.6: Droplet falling on a fluid film

Depending on the Weber number in an experiment, one will observe several different outcomes. Droplet-droplet collisions have been studied in great detail (see Jiang et al. (1992), Orme (1997)), and different outcomes have been identified. The droplet-film collision has not been studied to the same extent, but similar outcomes, namely bouncing, coalescence, partial coalescence and splashing have been observed (see Pan and Law (2007), Rein (1993), Zhao et al. (2011a))

One very interesting phenomenon observed experimentally is a droplet floating on a fluid film for several seconds before coalescing, see Jones and Wilson (1978), Couder et al. (2005). This is not something that has been successfully simulated numerically, and is one of the phenomena this thesis will try to obtain. Zhang et al. (2009) observed another interesting phenomenon, a "second-stage" partial coalescence that also have been observed at NTNU (Thermal Two Phase Flow Laboratory (2013)). This phenomenon involves a droplet partially coalescing, the second droplet partially coalescing and so on. Figure 2.7 summarizes the most likely outcomes of low to medium We number collisions. Higher We numbers are usually associated with splashing, and will not be covered in this thesis.
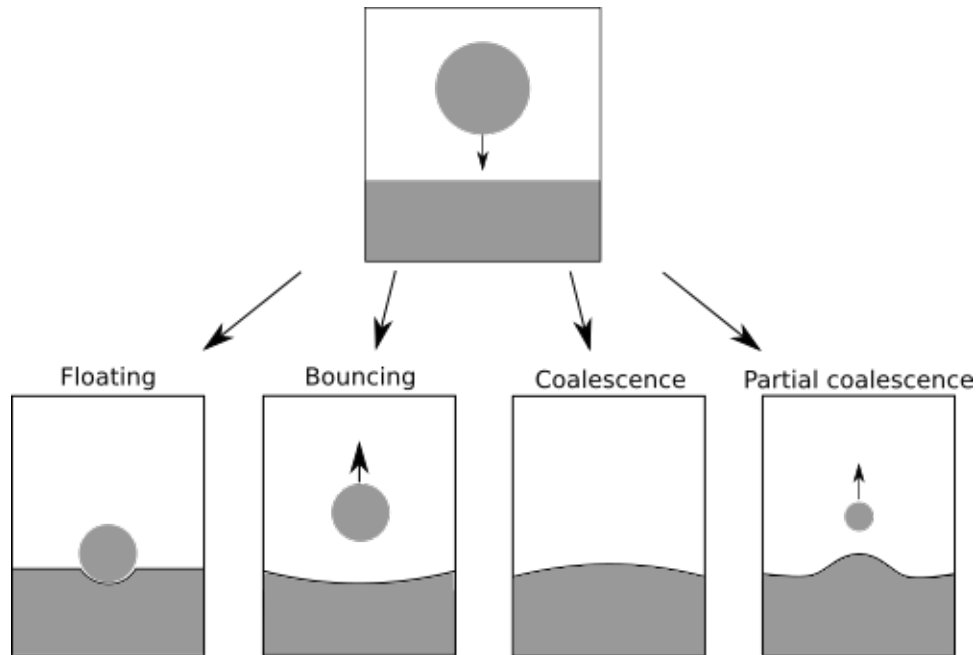
Figure 2.7: Low to medium Weber number outcomes

Collision Outcomes

The following section will cover some of the physics regarding the different collision phenomena. Starting with bouncing. The reason why a droplet can bounce on a liquid surface is due to the fact that there is a thin fluid layer between the droplet and the film, see figure 2.8.
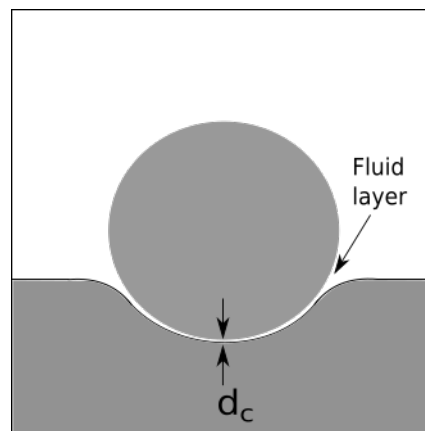
Figure 2.8: Fluid-film suspending a droplet

The inertial forces in the falling droplet will drain the gas film away. Define the critical interfacial distance as d_c. If the two fluid surfaces are further separated than d_c when the translational momentum of the droplet is lost, the surface tension in the film will act to bring the film

to its original shape, and the droplet will bounce.

If the two fluid surfaces are closer than d_c, the surfaces will merge. Interestingly this merging can occur at both higher and lower Weber number than the bouncing outcome Zhao et al. (2011b). If the Weber number is low, the floating phenomenon may be observed. Small inertial forces in the droplet does not deform the film to the extent that the reversal surface forces can overcome the gravitational forces acting on the droplet, and the droplet floats. The droplet is suspended by the surface as the gas film is slowly drained away. When the separation is sufficiently small, the Van der Waals forces are starting to apply (Qian and Law (1997)). The van der Waals forces are weak intermolecular forces that can attract or repel, and are not based on electrostatic interaction. The strength and range of the force depends on whether the fluids are permanent or induced dipoles, as a consequence, the critical distance d_c is highly dependent on what fluid is used. Different sources report critical distances in the range of $d_c = 0.1 - 100 \mu m$ (Couder et al. (2005), MacKay and Mason (1963), Jones and Wilson (1978), Gilet and Bush (2012)).

The critical interfacial distance can be reached using a high Weber number as well. In this case the inertial forces in the falling droplet is large, and the intermolecular forces do not affect the coalescence. This was experimentally observed by Zhao et al. (2011a). An even higher Weber number will cause fragmentation and will not be covered in this thesis.

The drainage of gas can be accelerated or slowed down in several ways. One way of slowing the process down is if the film is heated, and you observe a phenomenon similar to the Leidenfrost effect. The Leidenfrost effect is characterized by vaporization of a liquid to create a protective gas film. This thesis however, will not take any thermal considerations into account. Having a thin liquid film will act as an accelerator of the drainage of the protecting gas. This is because the wall is immovable, and the effect of the impact forces will be larger.

Other factors influencing the drainage of the protective gas are the densities and viscosities in the simulation. Simulations show that a heavier gas needs more momentum to be expelled. This will widen the Weber number interval where bouncing is observed. The same is true for high viscosity fluids.

This thesis will cover vertical collision between a falling droplet and a same-liquid film. The liquid film will be thick. Thick film, or deep water pools is defined as the film thickness h_f (figure

2.6) where the bounding solid surface no longer influences the behaviour of the falling droplet. In the literature, this thickness is not universally defined. In the work of Vander Wal et al. (2006), a pool/thick film was defined as 10 times the droplet diameter. Pan and Law (2007), in a more scientific approach using the energy budget, reports a thickness of ≈ 2.5 times the droplet radius as the deep-pool limit. Define H_f as the ratio of film thickness to droplet radius:

$$H_f = \frac{h_f}{R} \tag{2.33}$$

Pan and Law (2007) discovered that the droplet behaviour upon impact is dependent on the Weber number and H_f. The dependence on H_f disappeared when the film was sufficiently thick. Due to the limitation of this thesis, the H_f will be reasonably high (≥ 2.5), and the collision outcome should therefore predominantly be dependent on the Weber number.

2.4.1 Numerical Simulation

As seen in the above sections, some experiments on droplet-film collisions have been performed, and we have a reasonable understanding of the physical phenomena. Numerical simulations have not been performed to the same extent. Three numerical methods have been proposed:

- **The front tracking method** (Tryggvason et al. (2001)), where the interface is tracked by following certain control points.

- **The continuum surface force model (CSF)** (Brackbill et al. (1992)), where the surface tension is expressed through the gradient of the continuum variable and the field curvature.

- **The phase-field method**, as described in section 2.2.

The CSF method can be implemented using, among others, a level-set method or a volume of fluid method (Tanguy and Berlemont (2005), Scardovelli and Zaleski (1999)). Of the three, the phase-field method is the only one based on the free energy of the system (section 2.2), not the surface tension forces.

The problem with numerical simulations of droplet-film collisions is topological changes like coalescence or breakup. The solution has in many cases been to manually remove or merge the surfaces to artificially induce coalescence (Nobari et al. (1996), Pan and Law (2007)). This

procedure has often been preceded by an experimental investigation to obtain the point of co-alescence. This method is clearly not valid for simulation, as you need ad-hoc information. Pan and Suga (2005) using a level-set method, successfully simulated both the high-energy co-alescence and the bouncing regime of droplet-droplet collisions, but failed to simulate the low-energy coalescence that are believed to originate in intermolecular forces. This phenomenon is yet to be solved numerically. Implementing the phase-field approach is hopefully a step towards solving this problem, since no ad-hoc information is needed and the model describes interface coalescence based on energy minimization arguments.

Another argument for using the phase-field approach is the lack of discontinuities and delta functions. The calculations can also be made on a fixed grid, as opposed to sharp-interface methods, where the grid generally have to follow the interface. The numerical process is there-fore greatly simplified.

2.4.2 Deep-pool experiments

This section will cover, in more detail, the experiments on deep-pool collisions performed by Zhao et al. (2011b). The experimental focus was on the transition between bouncing and coa-lescence of droplets on deep liquid pools, and this work will be used as the main reference in this thesis.
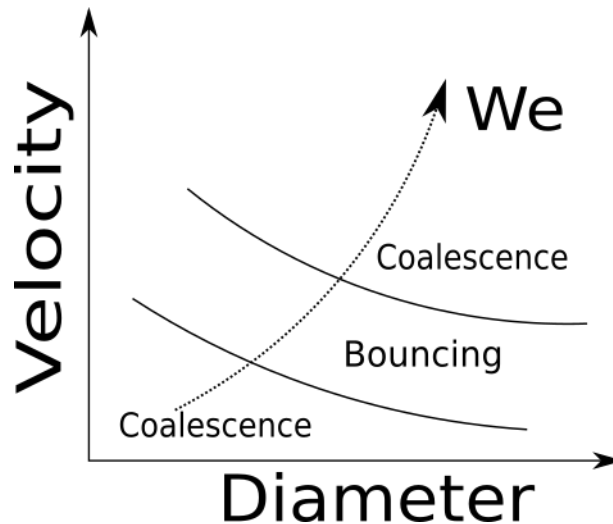

Figure 2.9: Low to medium Weber number outcomes

Several interesting discoveries were made. Coalescence was discovered at both low and high

energy collisions, with a bouncing regime in between, see figure 2.9. Typical Weber numbers of bouncing was We≈ 5 − 15. During coalescence, a "neck" will form, and depending on the vertical and horizontal collapse of the neck, a secondary droplet may pinch off. This partial coalescence was observed as a transitional region between both high and low energy coalescence and bouncing.

The bouncing region is characterized by deformation of both the surface and droplet, before the surfaces restitute and the droplet bounces. In the bouncing regime, the mass is conserved, however momentum is lost. The coefficient of restitution $c_r = \frac{|V_2|}{|V_1|}$ is used as a measure of conservation of momentum, and is approximately constant over a large range of Weber number, however at low We this coefficient increases sharply towards the upper limit of 1. It was observed that high viscosity and high surface tension increases the coefficient of restitution.

The contact time during bouncing was found to be independent of impinging velocity, given a constant diameter. A time scale can be made using the parameters in the experiments,

$$\tau^* = \sqrt{\frac{\rho D^3}{\sigma}} \tag{2.34}$$

The contact time can be expressed as $C\tau^*$, with C being C=1.72. The contact time can be separated into three stages, deformation, oscillation and restitution. It was observed that the restitution process is slower than the deformation process in the bouncing regime. Experiments using different liquids and velocities showed similar results.

A model for the transition between bouncing and coalescence was proposed (Zhao et al. (2011b));

$$K = We \cdot Oh^{-0.58} \tag{2.35}$$

with K=43 for low energy transitions, and K=119 for high energy transitions. Oh is the Ohnesorge number:

$$Oh = \frac{\mu}{\sqrt{\rho D \sigma}} \tag{2.36}$$

Equation 2.35 will be used frequently to identify the different collision regimes.

Chapter 3

Case Studies

This chapter will cover the methodology, settings, goals and objectives in the simulations performed. In the first section, the Cahn-Hilliard equations will be used to simulate phase separation into one or two droplets. In the second section, the CH and NS equations are coupled to simulate cases of falling droplets.

The Cahn–Hilliard equations are solving for the development of the order parameter ϕ. Solving for the order parameter should give a distribution with a thin, but finite interval where the parameter changes sharply, but continuously. Optimally, the distribution is symmetrical and strictly increasing/decreasing, with no oscillations, see figure 2.2b. The domain needs to have a sufficiently fine resolution for this to be achievable. An important dimensionless number that relates the interface parameter ϵ to a characteristic length is called the Cahn-number. Several definitions can be made, and the following will be used in this thesis:

$$Ch_L = \frac{\epsilon}{\Delta x} \tag{3.1}$$

where $\Delta x = L/(Ne \cdot P)$ is the size of the average numerical cell, L is the domain length, Ne is the number of elements and P is the polynomial expansion; and

$$Ch_r = \frac{\epsilon}{r_0} \tag{3.2}$$

where r_0 is the initial droplet radius. One of the goals of this thesis is to investigate what resolu-

tion (Ch_L and Ch_r) is needed to obtain a satisfactory solution.

Another numerical factor in this particular solver is how the degrees of freedom (dof) are increased. In the spectral element method, there are two ways of increasing the dof, increasing the polynomial expansion order P, or the number of elements Ne. Increasing the polynomial order is known to give more accurate results, and show better convergence rates (section 2.3.1). The computational cost, however, is larger. As a practical approach, increasing the number of elements at a moderate polynomial expansion will be employed in this thesis.

3.1 Droplet Equilibrium

This section will simulate the phase-separation into a droplet and a surrounding fluid. There will be no convective terms. The uncoupled Cahn–Hilliard equation implemented in this section is as follows:

$$\frac{\partial \phi}{\partial t} - \frac{M}{Pe}\Delta\mu_0 = 0 \tag{3.3}$$

$$[\phi^2 - 1 - \epsilon^2\Delta]\phi - \mu_0 = 0 \tag{3.4}$$

The initial and boundary conditions listed in figure 3.1. The gradients of the order parameter and the chemical potential is zero in the outward direction, along all boundaries. All other settings can be found in appendix A. Note that the definition of the free energy, eq. 3.4, is slightly different from what was defined in the theory chapter, this definition follows from defining $\phi = [-1,1]$, $\psi(\phi) = (\phi^2 - 1)^2/4$, and including the constant parameters α, σ in μ_0.

3.1.1 Single Droplet Equilibrium

A single droplet is simulated using conditions in figure 3.1. The goal of the simulation is to see whether the solver is successful in simulating a droplet using the Cahn–Hilliard equations, and if so, investigate the effect of changing the Cahn numbers Ch_L and Ch_r.

$$\frac{\partial \phi}{\partial \vec{n}} = \frac{\partial \mu_0}{\partial \vec{n}} = 0,$$

on all boundaries
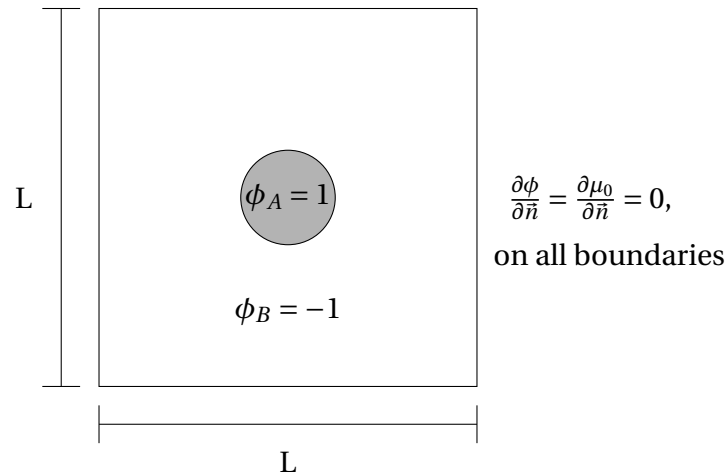
Figure 3.1: Boundary and initial conditions, Single Droplet Equilibrium

3.1.2 Two Droplet Equilibrium

The initial field is manipulated to simulate two droplets, see figure 3.2. The boundary conditions are as previously shown. The non-convective Cahn–Hilliard equations are globally conservative. The goal of this simulation is to investigate whether it is possible for mass (ϕ) to shift from one fluid body to another, with no convective terms.
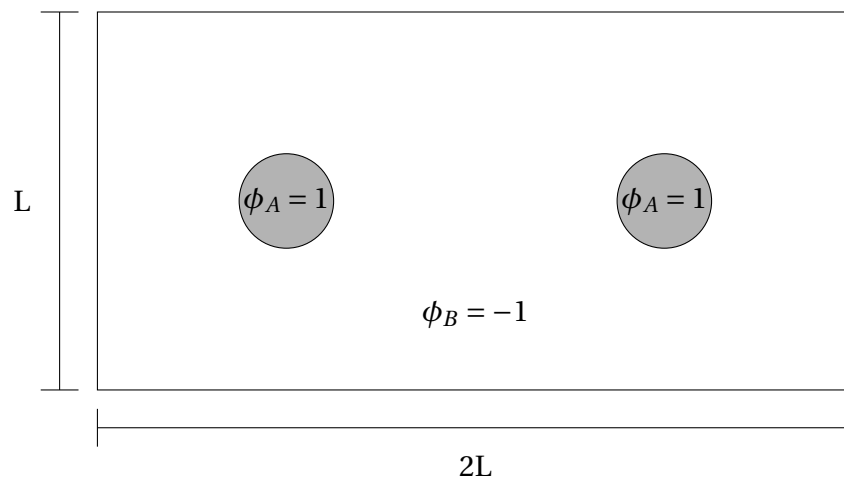
Figure 3.2: Initial conditions, Two Droplet Equilibrium, boundary conditions as in figure 3.1

3.2 Falling Droplet

The Cahn–Hilliard and Navier–Stokes equations are coupled to solve dynamic multiphase problems. In this section, the set of equations, 2.7-2.10 is solved. The initial and boundary conditions are presented in 3.3. Two phases with $\phi = \{0, 1\}$, no slip, no penetration along all boundaries, as well as no flux of the order parameter or chemical potential. The mesh parameters in all simulations will be $Ne_x = 24$, $Ne_y = 48$, $\epsilon = 0.02$, $P = 4$, before refinement. All other parameters may be found in appendix A.


$$\vec{u} = \frac{\partial \phi}{\partial \vec{n}} = \frac{\partial \mu_0}{\partial \vec{n}} = 0,$$

on all boundaries.
Fixed pressure at
centrepoint on
lower boundary.
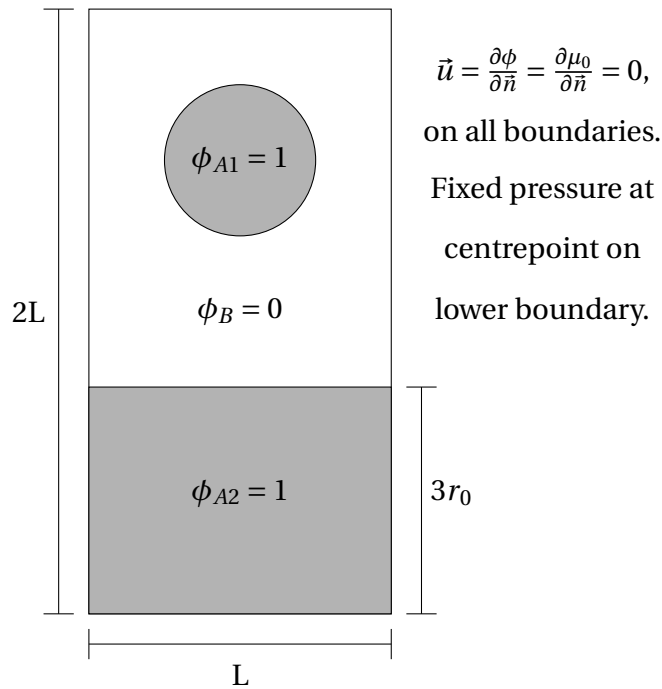
Figure 3.3: Boundary and Initial conditions, coupled CH and NS equations

The solver provided in the project was originally simulating a droplet falling on a solid surface ($\phi_{A2} = 0$). Using the original solver, a droplet falling on a solid surface will be simulated. The initial field and parameters will then be manipulated to simulate a droplet falling on a fluid film with the desired physical parameters. Lastly, specific experimental results will be copied. The reasoning behind changing the non-dimensional parameters can be found in appendix D.

3.2.1 Droplet Falling on Solid Surface

A droplet falling on a solid surface is simulated, this simulation will use the original parameters ($\phi_{A2} = 0$), and will therefore be referred to as **Simulation 0**. The objective is to look at the mass conservation, both locally in the droplet, and globally in the computational domain, as well as the dynamics in the simulation.

3.2.2 Droplet Falling on Fluid Film

In **Simulation A**, a fluid film is added to the domain. The physical parameters are kept as in simulation 0 to ensure a functioning simulation. The goal of this simulation is to see how the solver simulates the coalescence of two fluid bodies. The collision outcome will not be studied in detail, obtaining a functional simulation is the main objective.

In **Simulation B**, the non-dimensional numbers discussed in eqs. D.3-D.5 will be implemented based on a Weber number of $We \approx 10$. The density and viscosity ratios will be kept as in simulation 0 and A.

As a way of moving closer to specific experiments, we now present results from Zhao et al. (2011b). Table 3.1 shows the physical properties of 1-propanol and distilled water droplets falling in air. In both experiments, the droplets bounced on the liquid surface. D and V denotes the droplet diameter and impact velocity respectively. **Simulation C** will use the density and viscosity values from the 1-propanol collision.

Table 3.1: Bouncing Droplets, from Zhao et al. (2011b)

Fluid	ρ [kg/m^3]	μ [mPa/s]	σ [mN/m]	D [mm]	V [m/s]
1-propanol	799.6	1.968	23.28	0.24	1.14
Air	1.2	0.0186	-	-	-
Distilled Water	996.9	0.89	71.99	0.16	1.2
Air	1.2	0.0186	-	-	-

The next step would be to completely copy an experiment. Immediately, one discovers a problem. Looking at the 1-propanol collision, the droplet size is extremely small with respect to the impact velocity. A droplet of diameter $D = 0.24mm$ will need an initial falling height of $\approx 300D$ to obtain a velocity of 1.14m/s. That is not feasible if the collision is simulated numerically, due to the large computational time involved for a large domain. The attempts of replicating

experiments are therefore limited to simulating the regions described by equation 2.35 (figure 2.9), repeated for convenience below:

$$K = We \cdot Oh^{-0.58}$$

with K=43 for low energy transitions, and K=119 for high energy transitions. The physical properties of water (table 3.1) will be used to simulate one collision in the three following intervals; $K \leq 43$, $43 \leq K \leq 119$, $K \geq 119$, referred to as **Simulation D-F**.

Chapter 4

Results

4.1 Droplet Equilibrium

4.1.1 Single Droplet Equilibrium

Figure 4.1 shows the stable solution to the Cahn-Hilliard equation. The mass was found to be conserved both globally and locally in the droplet during the iteration process.
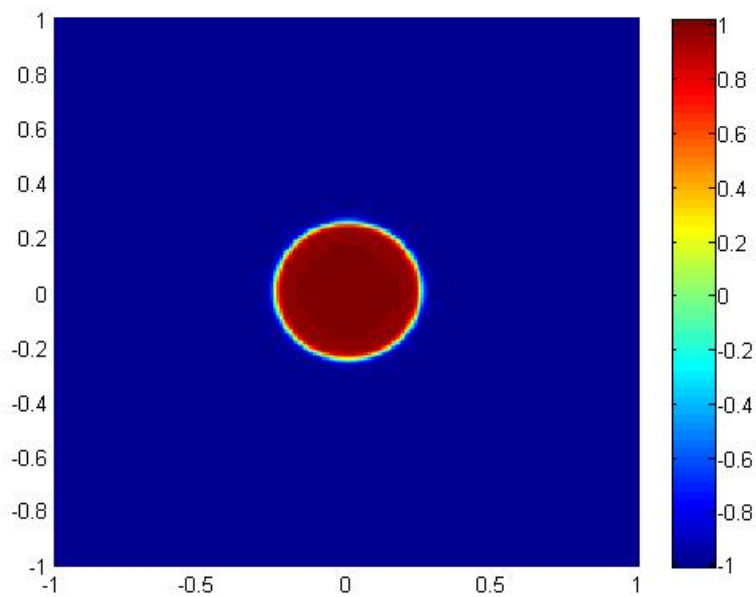

Figure 4.1: Cahn-Hilliard solution, ϕ. $\text{Ne}_x = 40$, $\text{Ne}_y = 40$, $\epsilon = 0.01$, $P = 4$

The numerical resolution, specifically the Cahn-number Ch_L, at a sufficiently resolved solution is listed in table 4.1 and figure 4.2. What simulations deemed acceptable are based on a visual inspection, and is therefore only used to obtain approximate guidelines, see chapter 5.

Table 4.1: Visually acceptable solutions

ϵ	Ne	P	Ch_L
0.05	24	4	2.40
0.02	16	4	0.64
0.01	32	4	0.64
0.005	40	4	0.40
0.0025	80	4	0.40
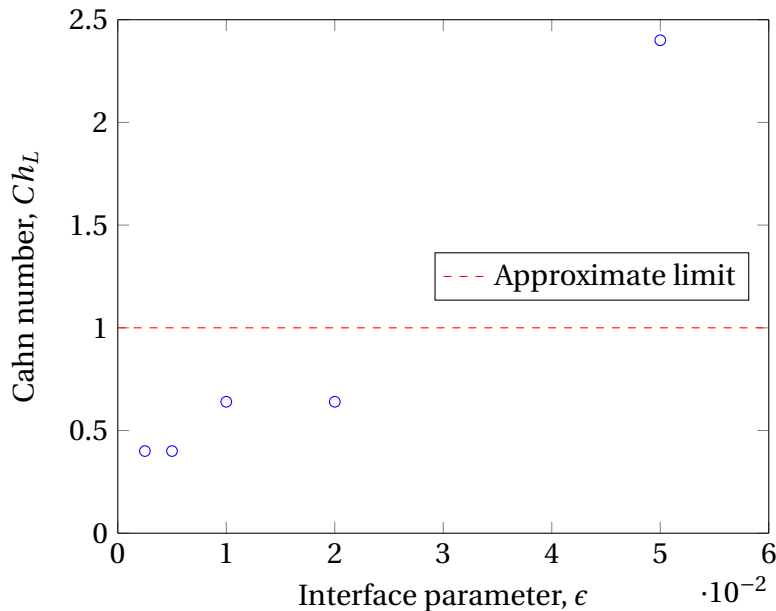
Figure 4.2: Cahn number needed for acceptable solution

The goal is to identify an approximate limit for how refined the mesh should be, to get a sufficiently resolved solution. This limit should be constant, i.e have the form $Ch_L = \frac{\epsilon}{\Delta x} = C$. If one disregards the first entry in the table, $\epsilon = 0.05$, then a reasonable limit seems to be $Ch_L = 0.5$, the interface parameter ϵ should be about half the width of the average numerical cell. Keep in mind, this is average numerical cell, and as will be explained in a later chapter, this is not representative for all simulations. Setting the limit to $Ch_L \geq 1$ is therefore recommended.

The first entry in table 4.1 was dropped due to the ratio $Ch_r = \epsilon/r_0 = 0.2$ being too large. For a properly resolved droplet to be possible, a limit of $Ch_r \leq 0.1$ is proposed, details in chapter 5.

4.1.2 Two Droplet Equilibrium

Two identical droplets were simulated. There was no change in mass, shape or size of the droplets during the iteration process. The hypothesis that mass loss, or shifting in mass, can only occur in simulations with a convective term, is assumed to be valid. Figure 4.3 shows the stable Cahn-Hilliard solution of two droplets.
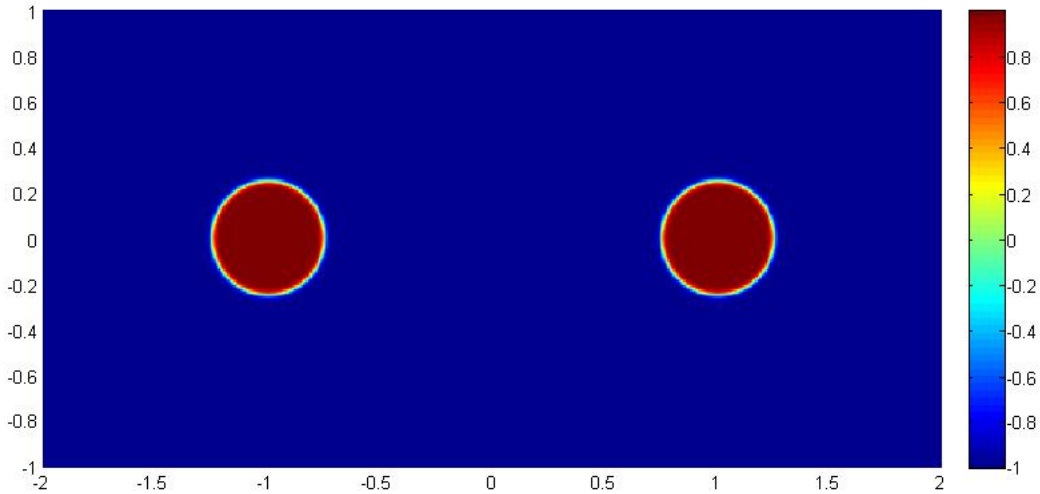
Figure 4.3: Cahn–Hiliard solution, ϕ. $\text{Ne}_x = 50$, $\text{Ne}_y = 100$, $\epsilon = 0.01$, $P = 4$

4.2 Falling Droplet

This section will present the results of the numerical simulations using the coupled Cahn–Hilliard and Navier–Stokes equations. Both droplets falling on solid and liquid surfaces will be presented, and compared with experimental results when possible.

4.2.1 Droplet Falling on Solid Surface

This section will present the results from simulation 0. Figure 4.4 shows the result of the simulation at evenly spaced timesteps. The Cahn numbers were $Ch_L = 1.92$ and $Ch_r = 0.08$, all other settings are listed in Appendix A. The acceleration of the centrepoint of the droplet is calculated to be close to the gravitational acceleration, when buoyant effects are considered. After impact,
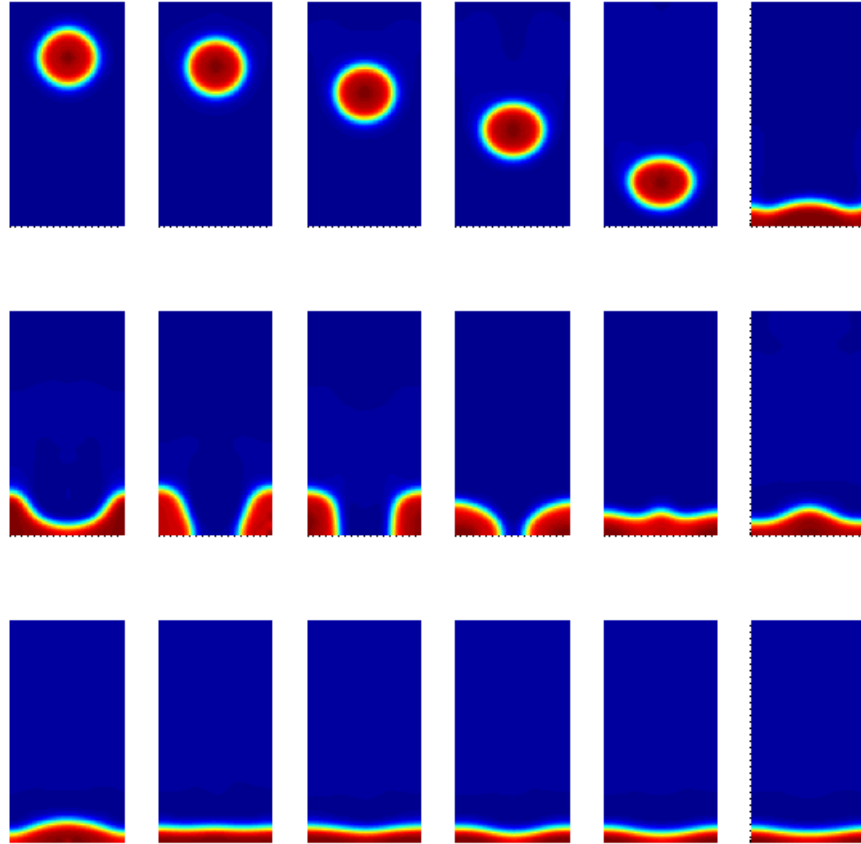
Figure 4.4: Simulation 0, t=[0 → 2.2]

the droplet separates into two droplets as the downward momentum is deflected outwards, and overcomes the surface tension in the film. The droplets eventually merge and the surface settles.

Figure 4.5 shows the velocity field $\vec{u}$ in the domain at times $t = \{0.3, 2.2\}$. The left snapshot displays the velocity field during the fall. There is a tendency that the surrounding fluid is escaping from underneath the droplet, recirculating up along the sides. This is exactly the dynamics one can expect in a closed domain. The velocity inside the droplet is almost uniform, another well modelled dynamic. At t=2.2 (right), when the film is settling, we see two pairs of counter-rotating vortices. The lower pair is created by the falling droplet, the top pair by the viscous effects and the bounded domain above. It may seem like there is a slight asymmetry in the position of the vortices, but this is due to where the velocity components have been drawn. In
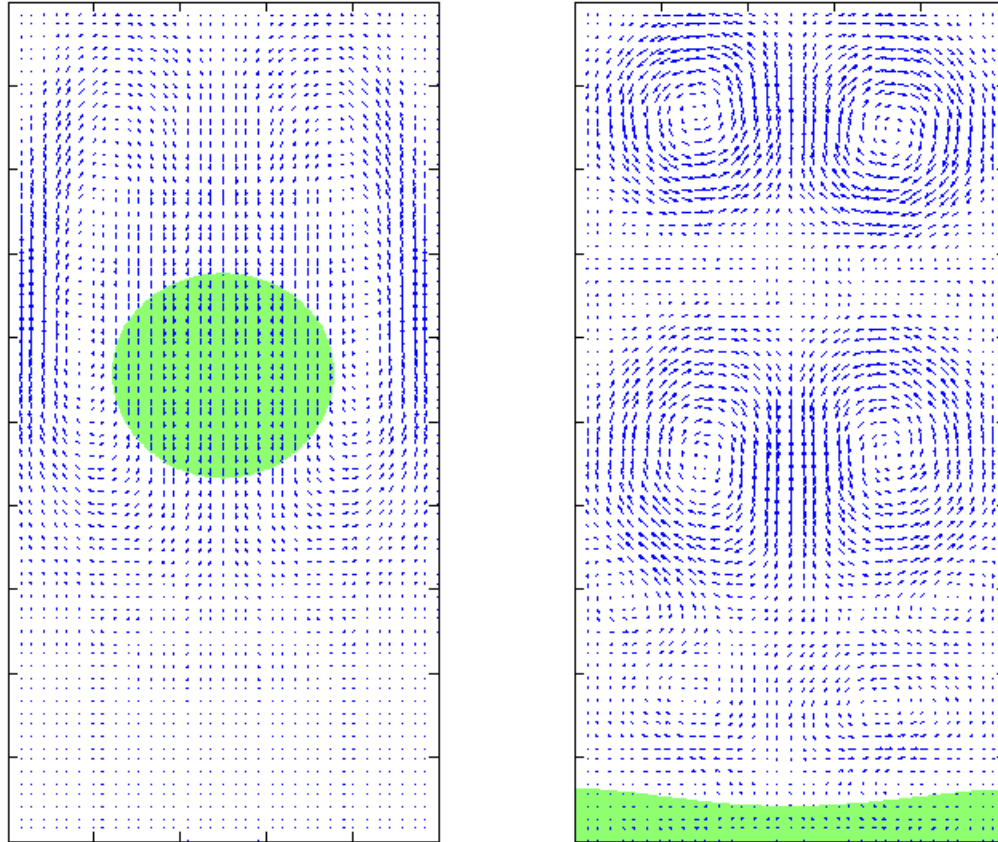
Figure 4.5: Velocity field, Simulation 0, t=0.3 (left), t=2.2 (right)

general, it seems like the dynamics of the droplet collision is modelled well. A huge problem with the simulation however, is the evolution of the mass in the system.

Figure 4.6 shows the development of the global mass in the simulation. Some regions can be identified; There is mass gain while the droplet is in free fall, there is mass loss at impact, and there is severe mass loss as the surface is settling. After about 2 seconds, the mass stabilizes, at about 75% of the original value. The non-conservative behaviour is concerning, especially coupled with the fact that refining the mesh 225%[1] did not change the behaviour noticeably.

---

[1]Percentage refinement from now on defined as follows: 50% more elements in both directions yields $1.5 \cdot 1.5 = 2.25$ times the number of elements $\rightarrow$ 225% refinement
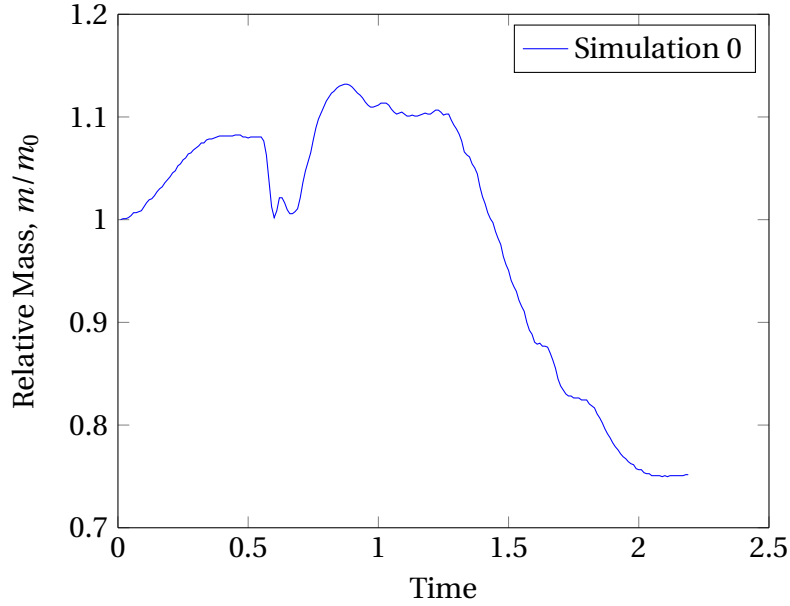
Figure 4.6: Global mass, Simulation 0

The Cahn number Ch_L

Several simulations using $Ch_L \approx 1$ were performed, none of the simulations worked. In all cases, the droplet was oscillating in space, seemingly without any gravitational effects. Figure 4.7 shows an example, simulation 0 using $Ch_L \approx 2$ and $Ch_L \approx 1$ respectively, otherwise equal parameters and grid resolution. Based on this, the guideline regarding the Cahn number Ch_L is revised to $Ch_L \geq 2$. A theoretical discussion can be found in chapter 5.
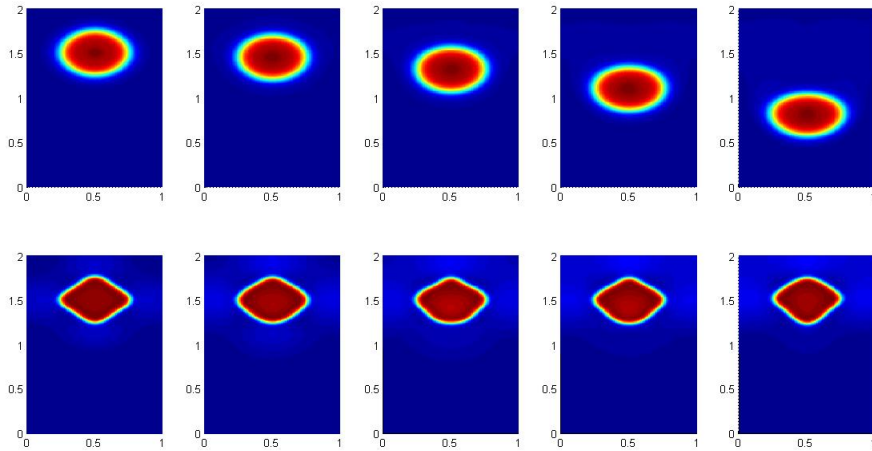
Figure 4.7: Simulation 0, $Ch_L \approx 2$(top), $Ch_L \approx 1$(bottom)

4.2.2 Droplet Falling on Fluid Film

This section will present the results from simulations A-F. In short, simulations A and B showed promising features in terms of the dynamics of the collision, however both displayed severe mass loss, similar to simulation 0. In chapter 5 various reasons are discussed and tested, without discovering the definite underlying reason. Simulation C also showed promising signs in terms of the dynamics of the problem, bouncing was observed, and more importantly, mass conserved. The local mass behaviour however, was not as desired. Simulation D-F was not successful. See figure 4.2 for an overview of the results.

Table 4.2: Simulation outcomes

Simulation	We[a]	Theoretical Outcome[b]	Outcome
A	19.6	Bouncing	Coalescence
B	5.3	Coalescence	Coalescence
C	9.2	Bouncing	Bouncing
D-F	-	-	No result

[a]Readers should be careful when calculating the Weber and Ohnesorge numbers based on generic parameters. The solver is only dependent on the viscosity and density ratios, not the actual values, however We and Oh is. Ex: $[\rho_1, \rho_2]$=[100,1] and [1000,10] is identical in the solver, but one order apart in terms of the Weber number.
[b]Eq. 2.35

Simulation A

Simulation A resulted in coalescence. The solver managed to merge the two fluid bodies to one, and the resulting film displayed similar movement and oscillation to what you would expect, before eventually settling. The big issue however, was the mass loss. The droplet itself had a small mass gain comparable to that of simulation 0 before impact. However, the global mass was reduced to about 75% of the original value after just 0.5 seconds. This is a problem, and something you should not observe in the CH equations. A global decrease and a slight droplet increase in mass also indicates that the main problem area is the fluid film. Refining the grid 225% did not improve the simulations, the dynamics was identical, and the mass loss was still present. After several non-successful simulations, settings A was suspended.

Simulation B

In simulation B, the arbitrary non-dimensional numbers, (Re, Bo), was changed to resemble a more physical setting. Figure 4.8 shows the results of simulation B. If one disregards the severe mass loss, then the outcome is clearly a functioning simulation of high energy coalescence, with large surface waves and no deceleration of the falling droplet. The Weber and Ohnesorge numbers was calculated to be $We \approx 5.3$ and $Oh \approx 0.057$, characterizing the impact as low energy coalescence. The simulation outcome is therefore not exactly as wanted.
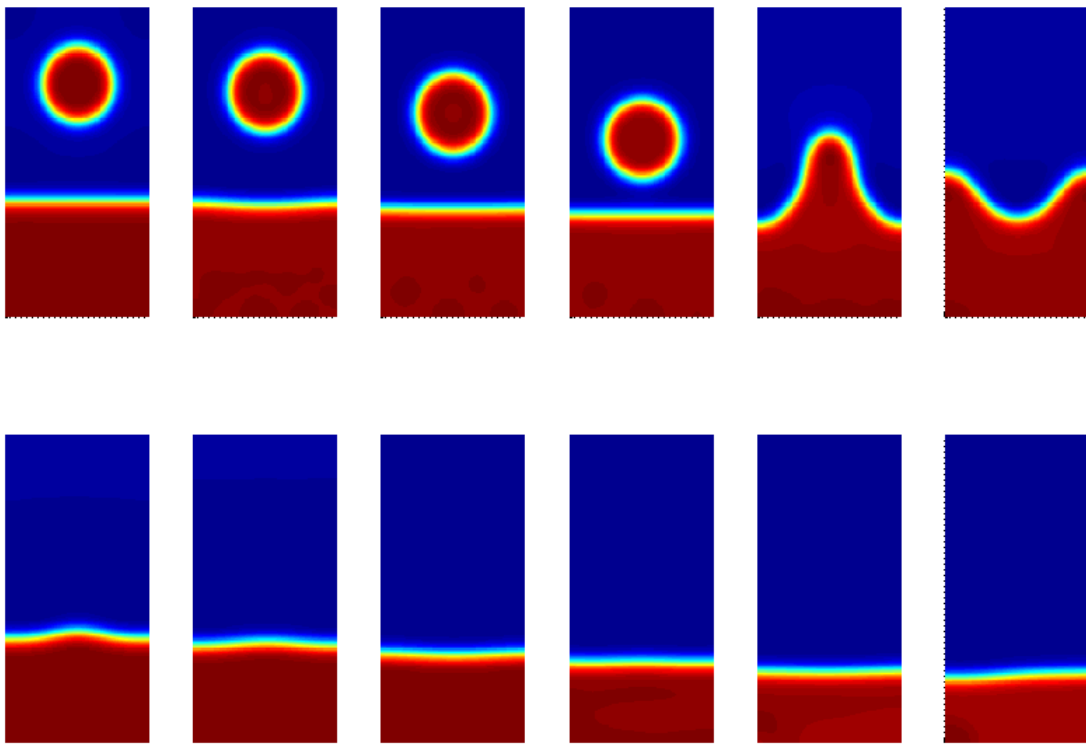
Figure 4.8: Simulation B, t=[0 → 1.25]

Notice the severe mass loss. Interestingly, the fluid film keeps on shrinking long after the impact. In 1 second, the mass dropped to about 55% of its original value. The droplet mass and size is approximately unchanged during the fall, and the mass loss is therefore occurring in the fluid film. The rate of mass loss in simulation A and B is roughly the same, differences in the initial few timesteps makes the total mass loss bigger in simulation A at any given time.

Simulation C

Due to the significant mass loss in simulation A and B, further attempts at getting closer to the physical setting was performed. Figure 4.9 shows the result from simulation C, where the density and viscosity ratios are taken from experiments. The Weber and Ohnesorge number was We≈9.3 and Oh≈0.029 yielding what should be a bouncing droplet. Keep in mind the concerns raised in the footnote of table 4.2 are still valid. There are some very promising signs, as well as some completely non-physical results. Two things immediately stand out, the mass loss in the droplet, and the apparent bouncing. This behaviour could also be observed in a partially coalescing droplet, but this possibility is discarded due to the lack of coalescence/neck-pinching dynamics. As of now, the outcome is classified as bouncing.

Figure 4.9: Simulation C, t=[0 → 1.1]

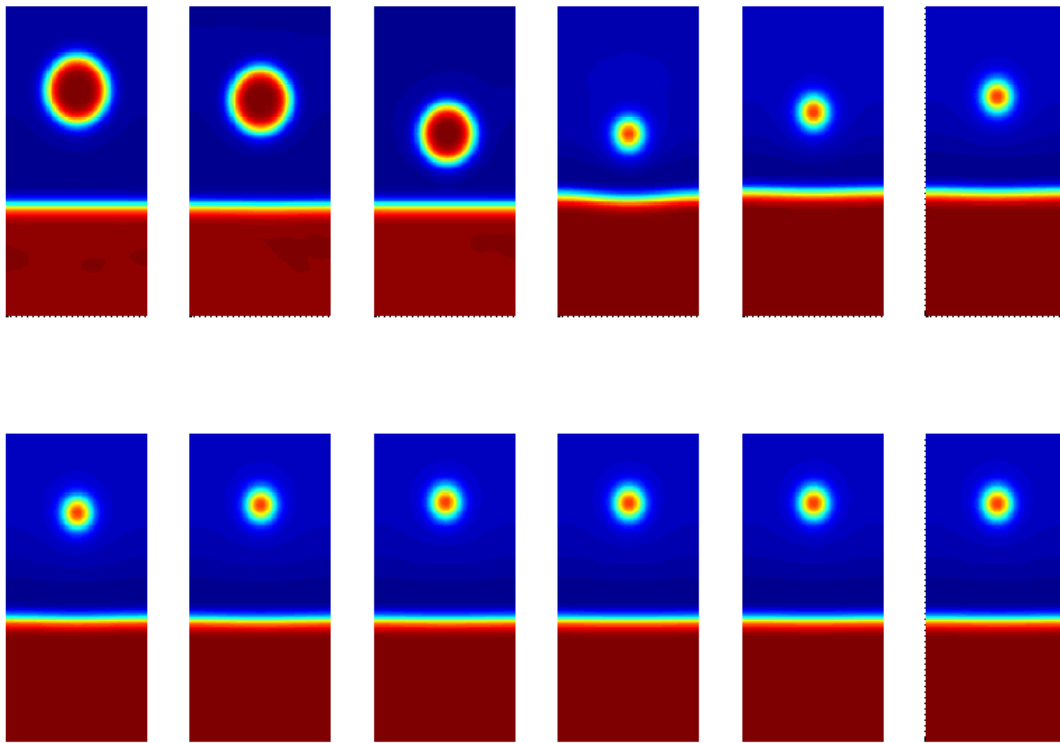Figure 4.10 shows the development of mass in the simulation. The mass is divided into droplet mass, film mass and global mass. There is severe mass loss in the droplet. However,

this only occurs before impact, then the mass of the droplet is constant. Similarly, the mass of the film is increasing around the time of impact, then stabilizing for the rest of the simulation. The decrease in droplet mass and increase in film mass perfectly offsets each-other, resulting in global conservation. The two effects are happening with a slight time shift, thus making the global mass "dip" before recovering. The settings used in simulation C is the first to obtain global mass conservation, a huge improvement on the previous sections. This change is thought to originate in the density/viscosity ratios, a thorough investigation will follow in chapter 5.
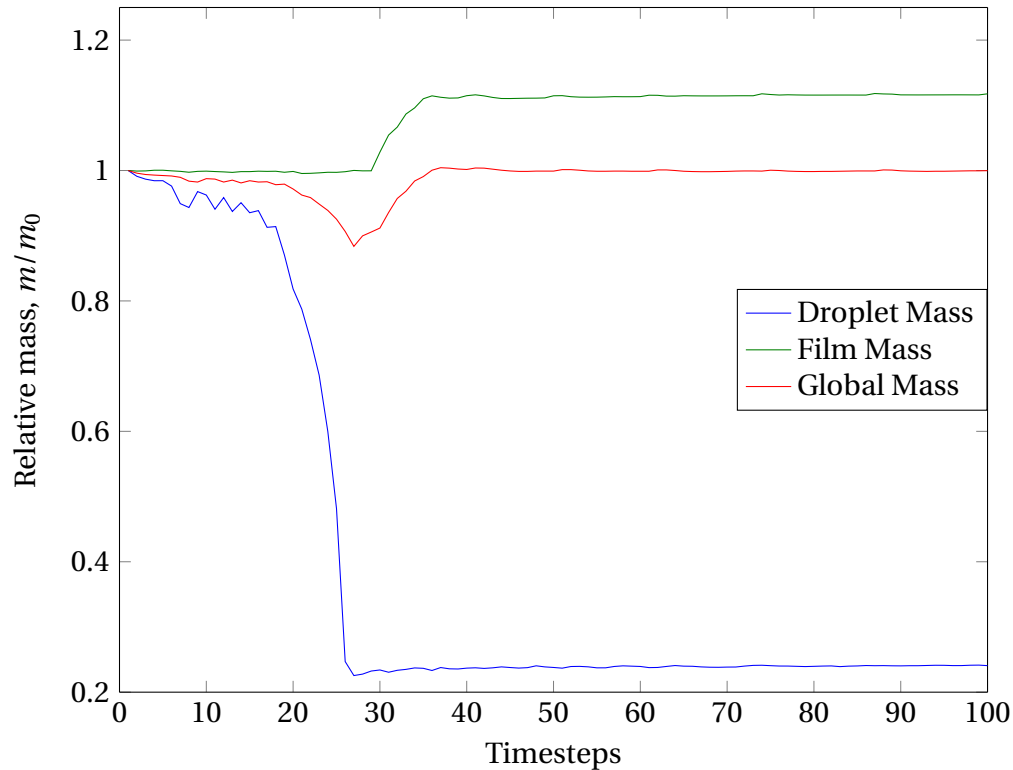
Figure 4.10: Mass distribution, Simulation C

Figure 4.11 shows the velocity field just before and just after the apparent bouncing. In the top row, during the fall, the velocity vectors are following the movement of the falling droplet. The bottom row is after impact. The velocity vectors are clearly moving downwards *through* the rising droplet. This should not be possible; it is as if the droplet is not there. Another aspect with this simulation is that the small droplet hovers in space after reaching its top-point (seen in figure 4.9). This effect may be attributed to an error in the code implementation, but this has not been identified yet.
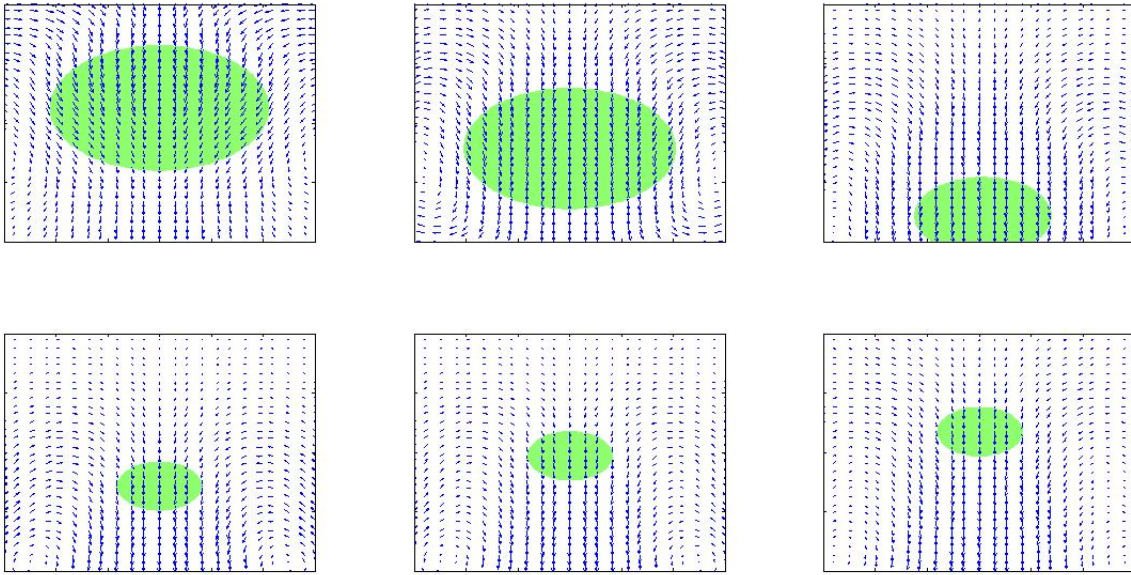
Figure 4.11: Simulation C, t=[0.05,0.15,0.25](top), t=[0.4,0.5,0.6](bottom)

Simulation D-F

Simulation D-F was not successful, possible reasons discussed in Chapter 5. Due to time restrictions, and further investigations into simulation A-C, no further simulations was performed using settings D-F.

Chapter 5

Discussion

5.1 Droplet Equilibrium

Figure 4.2 is based on a visual inspection, as it is difficult to quantify when the CH equations are properly solved. Figure 5.1 shows the cross-sectional view of the order parameter, solved using the same dimensions [L,r_o,ϵ]=[2, 0.25, 0.01], but different numerical resolution. Figure 5.1a is what you typically would regard as an unacceptable solution, and figure 5.1b is acceptable.

(a) Unacceptable distribution

(b) Acceptable distribution
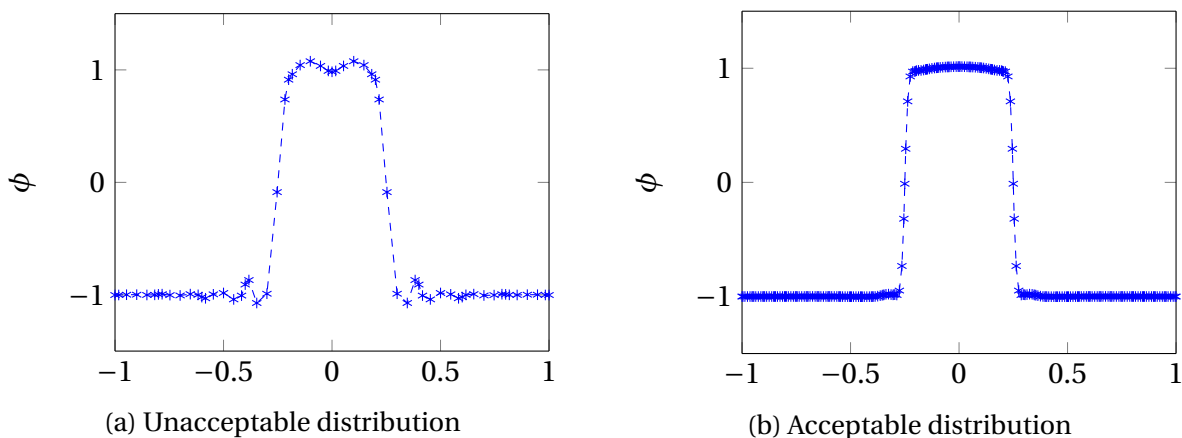
Figure 5.1: Visual inspection of order parameter ϕ

It is reasonable to believe that refining the grid would result in a better distribution of ϕ. This is not always the case in the current framework. A uniform grid is used in the simulations, but as seen in section 2.3.1, each element has a polynomial expansion. The solution will always be more accurate on the element boundaries, due to the basis functions, and less accurate within

the element. This effect becomes greater with a low polynomial order, due to the lack of bubble functions. Where the element boundaries are located with respect to the interface will therefore be important. This may lead to the paradoxical situation where refining the grid actually causes the region of interest, the interface, to be less refined, or not as accurately resolved as one could expect. Figure 5.2 shows a hypothetical situation where the number of elements increases from 2 to 3 (within the figure). The resolution in the area of interest clearly decreases.
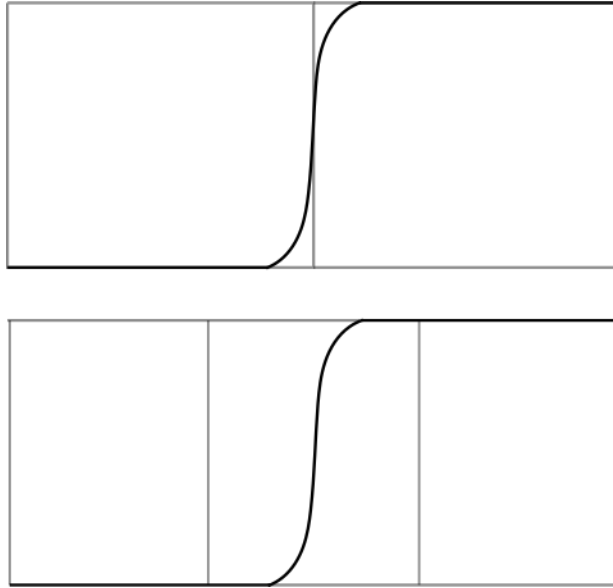
Figure 5.2: Possible effect of increasing the number of elements

A solution to the problem could be to place the element boundaries in the middle of the interface, to ensure a refined, and symmetrical solution. With the current geometry, this will equate to $Ne = 8n$, as $L/r_0 = 8$, with n being an integer.

Simulations using $\epsilon = 0.01$ and P=4, with varying number of elements supports this idea.

(a) Ne=32   (b) Ne=36   (c) Ne=40
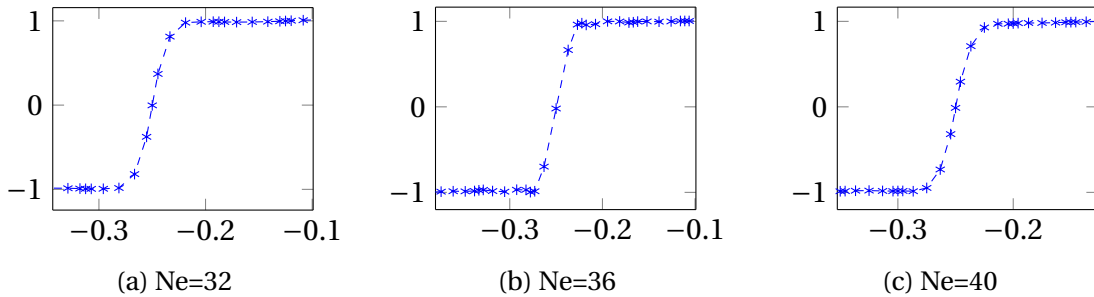
Figure 5.3: Order parameter ϕ, P=4, $\epsilon = 0.01$

Figure 5.3 shows the interface using Ne=[32,36,40]. Ne=32 and Ne=40 are multiples of 8, and it is clear by figure 5.3a and 5.3c that the interface is resolved better than in figure 5.3b (recall the analytical solution in figure 2.2b). The conclusion is that, if possible, use a number of elements that follow the $Ne = 8n$ rule. It is also clear from table 4.1 that all the entries are a multiple of 8, and thus, are following the "optimal" settings. When a droplet is falling, deformation and convection is introduced, and it is not possible to keep the droplet interface at the element boundaries. That is the reasoning behind increasing the limit to $Ch_L \geq 1$; it is recommended using an average numerical cell of the same size as the interface parameter.

The assumption of dropping the first entry in table 4.1 can be explained by the ratio $Ch_r = \epsilon/r_0 = 0.2$, the interface is too thick with respect to the droplet itself, and obtaining a properly resolved solution (ex. fig. 5.1), is difficult. This assumption can be investigated further by re-calling the analytical 1D solution, $\phi(x) = \tanh(\frac{|x|}{\sqrt{2}\epsilon})$. The derivative of the analytical solution is $\text{sech}^2(\frac{x}{\sqrt{2}\epsilon})/\sqrt{(2)}\epsilon$, which with $\epsilon = 0.05$ and $r_0 = 0.25$ yields a slope of ≈ 0.05 in the droplet centre. That is why it is difficult to obtain a visually satisfactory distribution with the parameters above. With the given initial radius, the slope at the droplet centre can be solved as a function of the interface parameter ϵ. A Cahn number of $Ch_r \leq 0.1$ yields close to no slope in the droplet centre, and a proper solution is possible. It should be pointed out that this recommendation is based on the non-convective CH equations, and does not take mass loss into account. Yue et al. (2007) recommends $Ch_r \leq 0.01$ if mass loss is to be negligible in the coupled set of equations.

5.2 Falling Droplet

Asymmetry

The preliminary results from simulation A revealed several errors. Figure 5.4 shows one of the early attempts, note both non-symmetric behaviour and severe mass loss.

The asymmetry was fixed by moving the reference point for the pressure boundary condition to the centrepoint of the lower boundary, at the symmetry line, see figure 5.5. No simulations showed any significant signs of asymmetry after this modification.
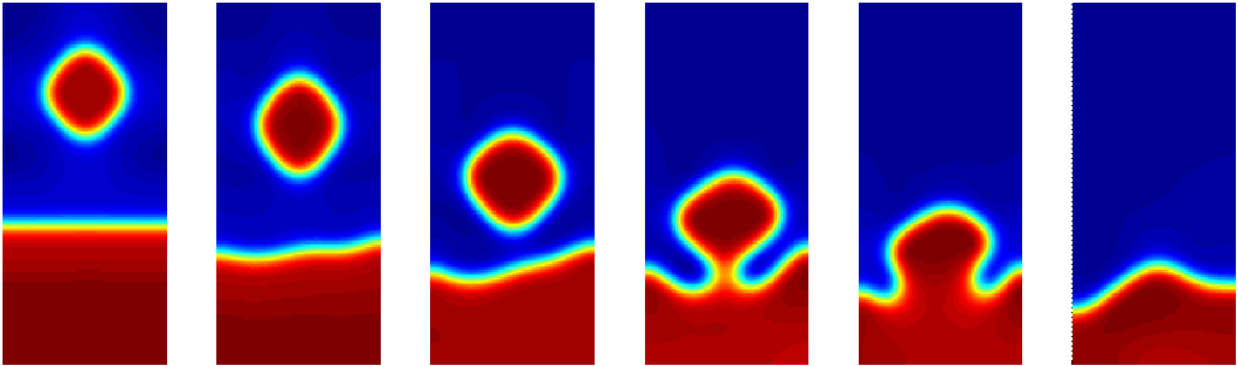
Figure 5.4: Asymmetry, Simulation A
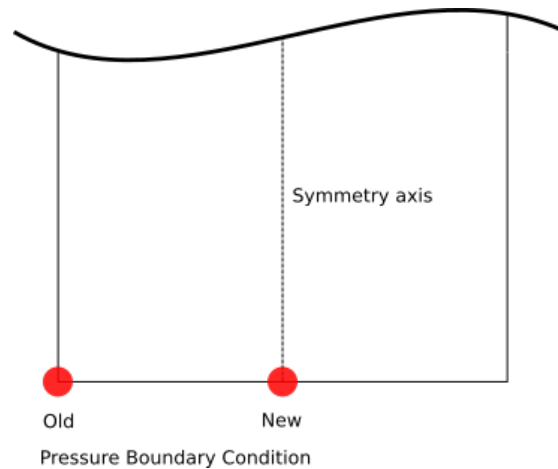
Figure 5.5: Reference point for pressure boundary condition

Cahn number

In section 4.2, the guideline limit for the Cahn number Ch_L was increased to $Ch_L \geq 2$ based on empirical evidence. No simulations using $Ch_L = 1$ worked, simulations using $Ch_L \approx 2$ did. A working simulation is here defined when the droplet is falling. The theoretical reason for this guideline-change is this: The solver simulating the Cahn–Hilliard equations alone is approaching a distribution of the following form, $\phi = \tanh(|x|/\sqrt{2}\epsilon)$. The solver simulating the coupled equations is approaching another form, $\phi = 0.5 + 0.5\tanh(|x|/2\sqrt{2}\epsilon)$. A Cahn number of $Ch_L = 1$ in the pure CH solution will cover the same percentage variation in ϕ as $Ch_L = 2$ in the coupled simulations. The two guidelines are therefore essentially the same. Regardless, this highlights the danger when transferring experiences from one solver to another.

5.2.1 Simulation A-C, Mass

The mass in the different simulations is behaving in a non-physical way. This is easily observed in figure 4.6 where the mass both increases and decreases significantly during different regimes of the simulation. Simulation A and B showed severe mass loss in fluid film, but relatively unchanged droplets, simulation C conserved mass globally, however not locally. This section will discuss some of the possible reasons for this behaviour and give results to some preliminary investigations into those reasons.

Mesh Refinement

An obvious source of error is a too coarse mesh. A refined mesh will usually produce a better result, however this is only the case if the problem and solvers are properly set up. In terms of the phase-field method, a thinner interface will also produce more accurate results.

Simulation B was repeated using a refined mesh. The interface parameter was reduced, and the number of grid elements was increased in such a way that the Cahn number $Ch_L \approx 2$ was approximately unchanged and Ch_r was reduced to 0.06. The new simulation had a 50% increase in elements in each direction, yielding a total of 2.25 times the degrees of freedom compared with the original simulation. By visual inspection, the two simulations had similar dynamics, the fluid film was still shrinking throughout. When looking closer at the results, the rate of mass loss was the same, differences in the first few timesteps caused the refined simulation to have a *higher* mass loss at any given time. Even further refinement of simulation B have not been performed. The same trend was observed when refining simulation A by 225%.

Parameter Study

One reason for the unpredictable mass behaviour may be the parameters used in the simulations. Table 5.1 lists some of the parameters used in simulations A-C, with drastically different outcomes. The surface tension and droplet diameter are of similar magnitude. There is presently no reason to suspect Re and Bo to affect the mass loss, especially when simulation C is located "between" A and B with respect to Re and Bo. The density ratio λ_ρ and, most notably, the viscosity ratio λ_μ is completely different, and may be a reason for the varying mass behaviour.

Table 5.1: Mass Conservation

Simulation	Outcome	λ_ρ	λ_μ	σ	r_0	Re	Bo
A	Loss	100	2	24.5	0.25	1000	100
B	Loss	100	2	24.5	0.25	55	10
C	Conservation[a]	666	106	23.28	0.12	111.5	19.4

[a]Global conservation. Mass shifted from droplet to film

In simulation A and B, the majority of the mass loss was occurring in the fluid film. One way of further investigate the reason behind the mass loss, is to simulate *just* a fluid film, with no falling droplet.

A fluid film alone was simulated. All settings as in simulation B. Figure 5.6 shows the evolution of the global mass in the system, and surprisingly, the mass is decreasing. There is mass
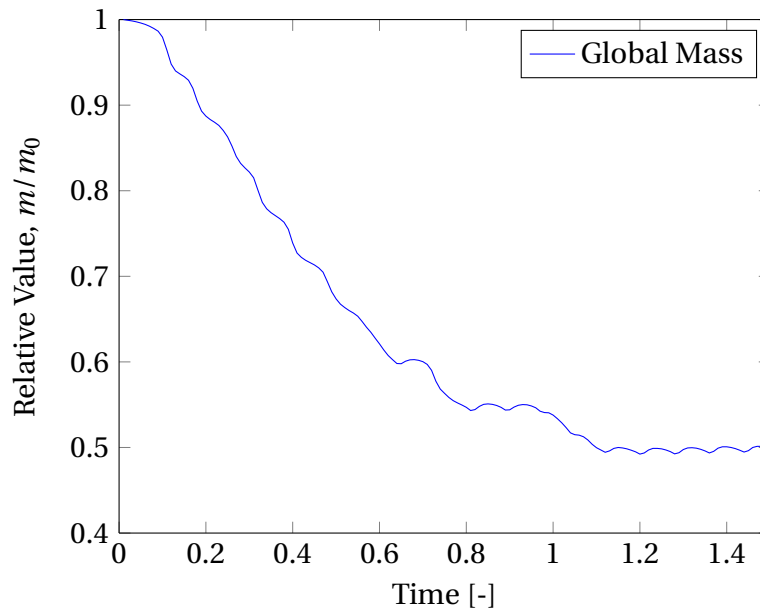
Figure 5.6: Mass of fluid film, Simulation B

loss even though there should be no movement in the entire domain. Furthermore, the mass loss is not linear or constant, but seems to oscillate. The fluid film does not completely vanish; the simulation stabilizes at approximately 50% of the initial mass. Refining the grid about 150% showed a similar trend.

A similar "film" simulation was set up using the parameters from simulation C. The mass was conserved to within 0.2% of the original value. This confirms that the mass conservation of

the fluid film, and indeed the whole domain, is highly dependent on the parameters used. It is also an indication of that the settings in simulation C may be a reasonable reference point going forward.

The main difference in simulation B and C is assumed to be the density and viscosity ratios. Two "intermediate" simulations were set up to investigate what ratio caused mass conservation, see table 5.2. I^ρ and I^μ denote intermediate simulations with "high" ratios of density and viscosity respectively, both simulations are a cross-combination of simulation B and C.

Table 5.2: Density and Viscosity ratios, Film simulation

Parameter	B	C	I^ρ	I^μ
ρ_1/ρ_2	100	666	666	100
μ_1/μ_2	2	106	2	106
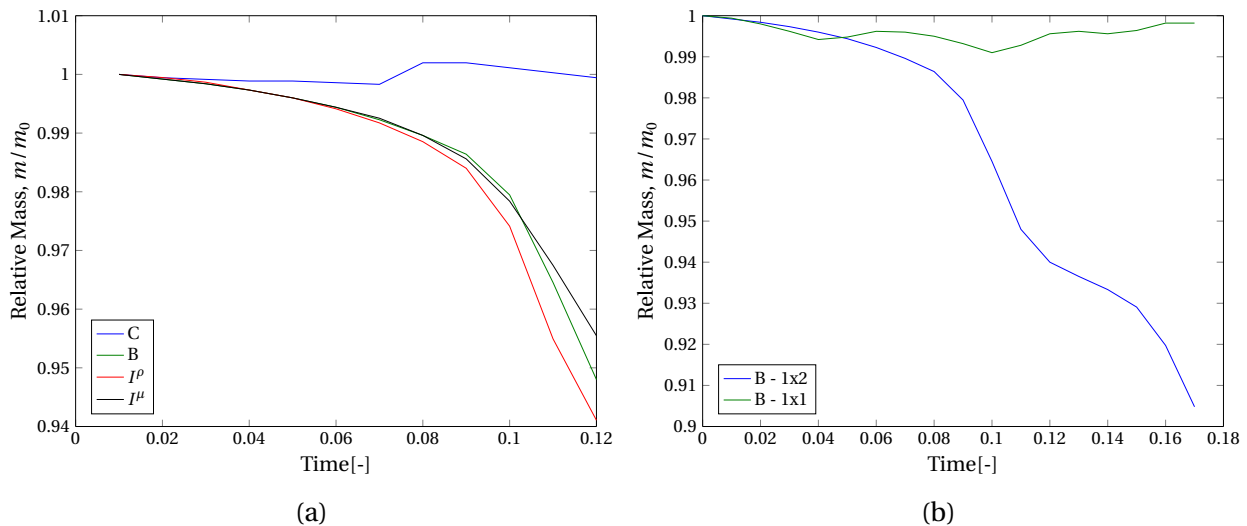
Figure 5.7: Mass of fluid film

Figure 5.7a shows the relative mass in the four simulations. No conclusions can be made on the importance of the density and viscosity ratios. Both ratios needed to be high for there to be mass conservation in the present simulations. One very concerning discovery was made when the pure film simulations were run on a 1x1 domain to reduce computational cost (recall original domain of size 1x2). All settings, B-C-I^ρ-I^μ conserved mass, example in figure 5.7b where settings B is plotted for different domain size. This indicates a missing Jacobian in the implementation. Further work is recommended.

Boundary Conditions

The boundary conditions imposed on the domain may be a significant source of mass loss. The boundary condition are as follows; no velocity at the boundaries, $\vec{u} = 0$, as well as no gradients in order parameter and chemical potential, $\frac{\partial \phi}{\partial \vec{n}} = \frac{\partial \mu_0}{\partial \vec{n}} = 0$. The conservation of mass was derived in chapter 2, eqs. 2.15-2.18. Note that the derivation is irrespective of the boundary condition $\frac{d\phi}{d\vec{n}} = 0$. We see that the simulations should conserve mass with the given boundary conditions. Simulations A and B however, showed severe mass loss and everything suggests that the mass loss is mainly occurring in the fluid film.

There are two primary physical ways of losing mass, convection and diffusion. First we are looking at how the no-penetration condition is upheld in simulation B, as this is controlling the convective mass loss. The velocities across the left and right boundary are small ($\sim \mathcal{O}(10^{-6})$), and positive (positive direction defined as outward). The velocity across the lower and upper boundary is larger, $\sim \mathcal{O}(10^{-4})$, and the largest velocities is always observed at the bottom. Figure 5.8 shows the time averaged velocity across the lower boundary. Note the peak velocity at the symmetry line. No special behaviour seen at the three-phase contact line (wall/film/gas).
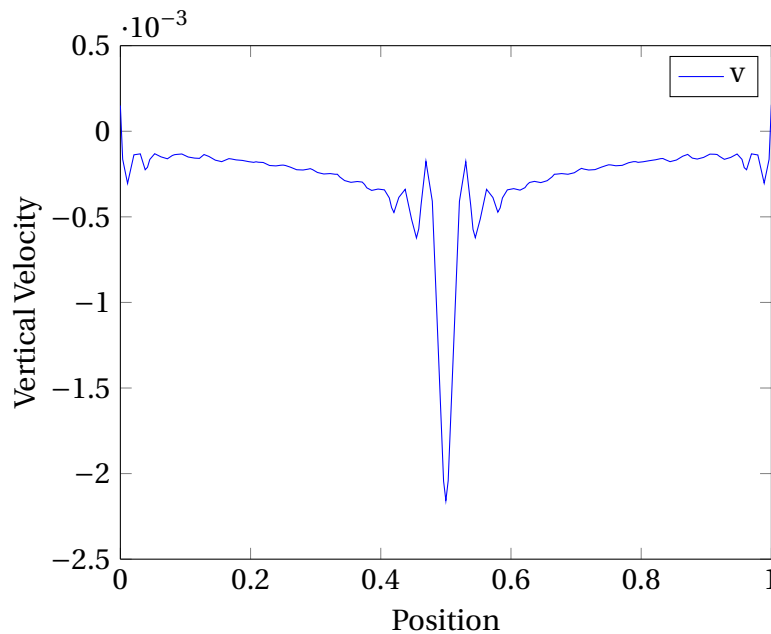

Figure 5.8: Time-average vertical velocity along bottom, Simulation B

Recall the convective term from the Cahn–Hilliard equation:

$$\int_\Omega \vec{u} \cdot \nabla \phi = \underbrace{\int_\Omega \phi (\nabla \cdot \vec{u}) d\Omega - \int_{\partial\Omega} \phi \vec{u} \cdot \vec{n} d\partial\Omega}_{\text{By Divergence Theorem}} \quad (5.1)$$

We are interested the last term of eq. 5.1, the flux along the boundaries. From the velocity and ϕ- field in the simulation, the convective mass loss was calculated to be $\Delta m = -4.6 \cdot 10^{-4}$. This is about 0.05% of the initial mass, and thus not the reason for the severe mass loss. The same procedure was repeated for the diffusive term:

$$\int_\Omega M\Delta\mu = \underbrace{M \int_{\partial\Omega} \nabla\mu \cdot \vec{n} d\partial\Omega}_{\text{By Divergence Theorem}} \quad (5.2)$$

There is no output M or $\nabla\mu$ from the solver. However, $\nabla\mu$ was calculated using backward differences to be far from zero. Yet more worryingly, it was not symmetric. It is reason to believe this could be a source of great mass loss. The LSQ is a weak formulation, but deviations this big from the prescribed boundary conditions should not be present. One way of artificially avoiding this problem will be discussed shortly.

A final note regarding the boundary conditions. The fact that simulation C, using the same solver, but different input parameters, is conserving mass suggest that the boundary conditions is not the fundamental issue. It is still reason to further investigate the boundary conditions based on the errors found, however other sources of error should not be excluded.

Weights used in the minimization of the least squares functional

The spectral element method is creating a system of discretized equations that has to be solved. The least squares method is minimizing a functional made up by the integral of the squared residual in the domain. In this functional, there will be a term related to the boundary conditions. The least squares method is a so-called "weak-formulation" as it is minimizing the functional in a global sense, rather than strictly enforcing conditions along boundaries and elsewhere. The relative importance of each term when minimizing the functional can be manipulated as a way of "forcing" the solver to emphasize one or the other.

Simulations with changed weights in the minimization process have not yet been performed, but may be a way of dealing with the problem. This is not a recommended permanent solution, as it is not solving the main problem, namely *why is it mass loss?*

5.2.2 Simulation A-C, Dynamics

Surface Tension

Figure 5.9(top) shows in detail the point of impact in simulation B, and how the two fluid bodies coalesce. The time step is 0.01 seconds. In theory, there should be a pressure build-up in the fluid under the droplet, deformation of the fluid film and droplet, before the eventual coalescence. This is not observed in the figure, or in the similar plots of the pressure field (not shown). The numerical resolution might be too low for this to be properly resolved, and bouncing or floating may not be possible until this behaviour is observed. Refining the mesh 225% (5.9, bottom) showed early signs of a deforming fluid film just before coalescence, which is promising. It is believed that further refinement will improved on this result.
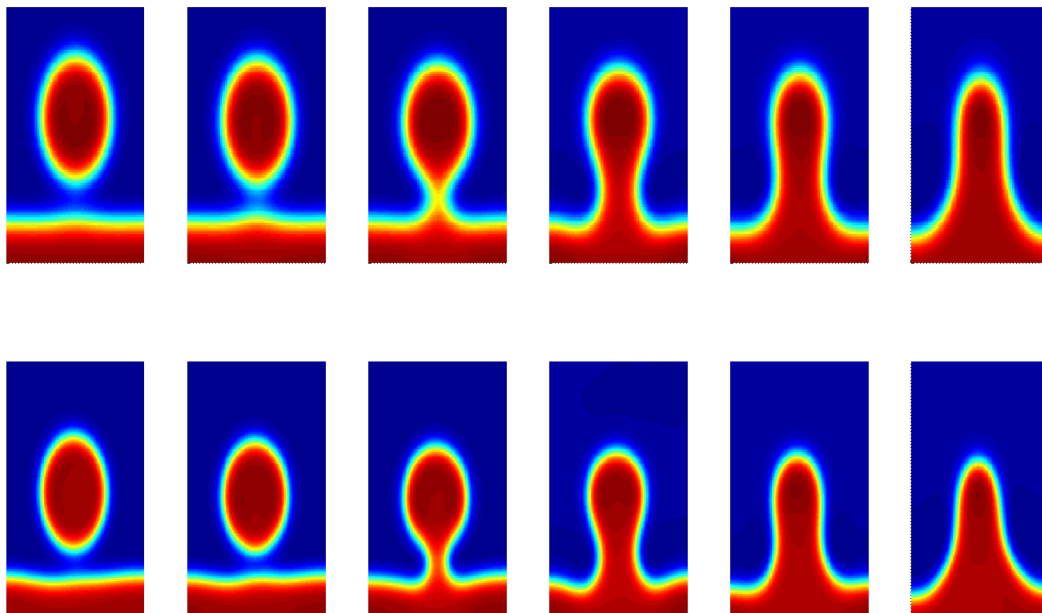

Figure 5.9: Simulation B, point of coalescence, $\Delta t = 0.01s$. $[Ne_x, Ne_y] = [24, 48]$, $\epsilon = 0.02$, P=4 (top), $[Ne_x, Ne_y] = [36, 72]$, $\epsilon = 0.015$, P=4 (bottom)

How the surface tension acts to minimize the energy of the system, in this case, minimize the length of the surface after coalescence, is modelled well. Figure 5.10a shows the position of the top of the droplet in simulation B. Before impact, an approximate quadratic path is seen, as it should be according to the gravitational acceleration. Then, just after impact, there is a drastic increase in the velocity of witch the top of the fluid is moving. This is the regime where the fluid bodies have coalesced, and the surface tension contracts the fluid film. This behaviour is also seen in the plots of the velocity field (not shown), where there is a distinct acceleration in the fluid just after coalescence. The last regime is when the surface is settling. Figure 5.10b shows a

(a) Simulation B   (b) Simulation 0
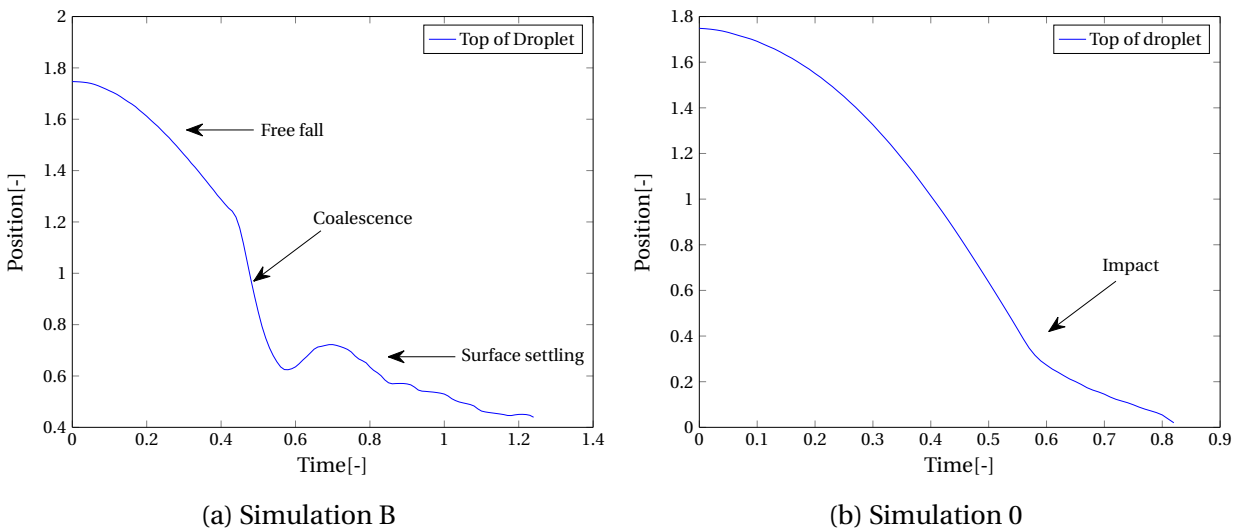
Figure 5.10: Coalescence and impact, Simulation B and 0

similar plot, for simulation 0. Observe the difference from simulation B. As theory suggests, the droplet is falling in an approximate quadratic way, until impact, where some of the momentum is lost, and the top part decelerates.

Simulation C

The apparent bouncing in simulation C is likely another phenomenon, not yet understood. The bouncing dynamics can be compared with the theoretical/experimental outcome to further investigate this. Figure 5.11 shows the centerpoint of the droplet during the simulation. Observe that the droplet bounces to a location *higher* than the original falling height, as well as losing 3/4 of its mass. Experimental results suggest a coefficient of restitution $c_r = \frac{|V_2|}{|V_1|} = 0.28$ for im-

pacts with the calculated Weber number (Zhao et al. (2011b)). This coefficient requires mass conservation in the droplet. The experimental bouncing behaviour is plotted in red. If the mass loss is factored in, and one assumes the same proportion of linear momentum conserved, the coefficient increases to $c_r = 1.17$, also plotted in figure 5.11. It is impossible to know how much linear momentum is retrieved when only a partial droplet is bouncing, and thus, the last plot is therefore not physically valid, but serves as an indication of the second bouncing height under those conditions. Buoyant and drag effects have not been included in this section.
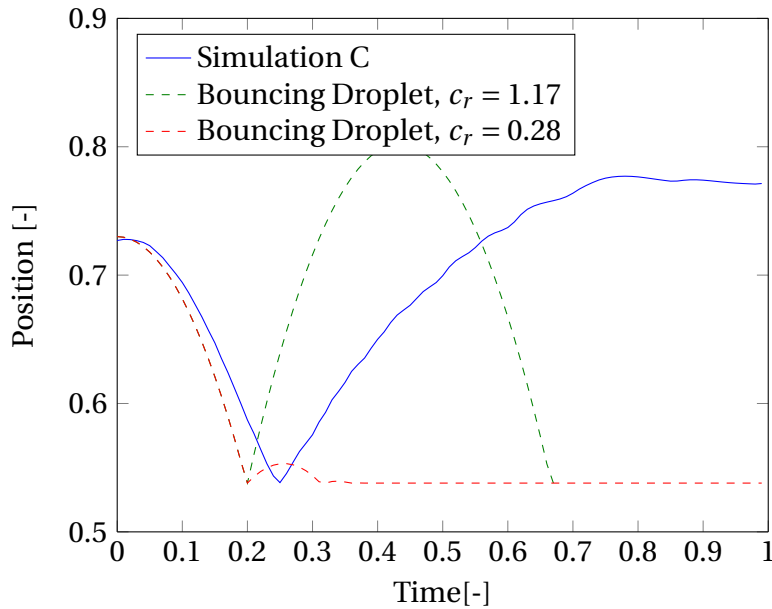
Figure 5.11: Bouncing droplets

5.2.3 Simulation D-F

The simulations using settings D-F were not successful. It is likely due to very small geometrical scales making the CFL number too big. The CFL number is the ratio of the convective length to size of the numerical cell. Due to time restrictions, no further attempts were made on copying experimental results, and this is left as recommended further work.

The Floating Droplet

One of the goals of this thesis was to simulate a droplet floating on a fluid film. To provoke this behaviour, a droplet can be placed just above the film. This will generate an almost negligible

impact velocity, and extremely low Weber numbers. This is essentially what was done in simulation D-F. As will be shown in the next section, care must be taken for this to be achievable computationally.

Consider a bouncing droplet. Zhao et al. (2011b) reports typical velocities of ≈ 1.5 for this collision outcome. Using classical mechanics, the initial falling height h can be approximated as $h = v^2/2g$. Note that this approximation is a lower limit, as it does not account for drag and buoyant effects, and the estimate will miss the desired velocity on the lower end. Using this approximation, the falling height should be $h \approx 0.11$. Figure 5.12 shows the separate 1D theoretical solutions of a film at a location $y_1 = 0.5$ and a droplet at $y_2 = y_1 + h$, using $r_0 = 0.25$ and $\epsilon = 0.01$, as this is the most commonly used settings in this thesis.
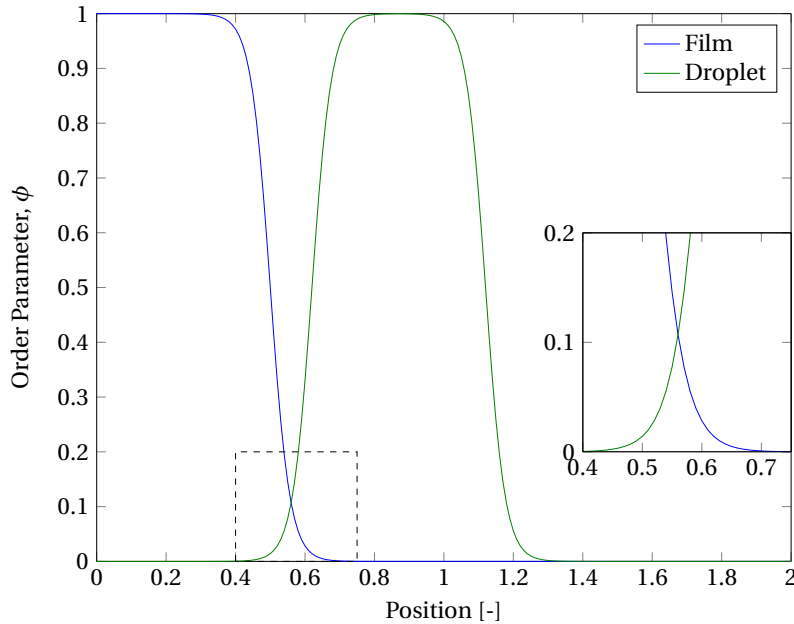
Figure 5.12: Overlapping interfaces

Observe that the distance between the film and the droplet is too small for the interface in both the film and the droplet to be properly resolved. There is a possibility that the solver is regarding the fluid bodies as merged even before the simulation starts. The reason why the solutions overlap, is the extent of which ϵ smooths out the interface. The interface parameter would need to be four times as narrow for this to be avoided at this separation. This would in turn require four times as many elements in all directions, and represent a dramatic increase in the computational cost.

The problem with "overlapping" interfaces can be avoided by using a larger initial separation of the two fluid bodies. By demanding the slope of the distribution of ϕ to be small in the film-droplet gap, one can calculate the minimum initial falling height where the solver manages to properly simulate the two fluid bodies. Based on a visual inspection, the height h should be no smaller than $h \geq 25\epsilon$.

Several simulations were performed using small droplet-film gaps, where the droplet lost its mass without falling. This was prior to setting a guideline of $h \geq 25\epsilon$, and it is believed that this may be one of the causes of the failed simulations.

5.3   Other

Time Consumption

The solver is written in Matlab, and is relatively time-consuming. Consider simulation B without refinement; $Ne_x = 24$, $Ne_y = 48$, $\epsilon = 0.02$ and P=4, using 16 nodes with 32 CPU's each on Vilje, a HPC supercomputer at NTNU. 125 timesteps (1.25s), was performed in 60 wall hours. That is pure simulation time, not considering time spent queueing. More information about computer specifications on Vilje can be found at NTNU (2016). Refining the mesh beyond this introduced significantly longer simulation time.

Due to computational cost, a complete refinement analysis and parameter study have not been achievable in the short timeframe, and is left as further work.

Chapter 6

Conclusion

6.1   Droplet Equilibrium

The Cahn–Hilliard (CH) equations are proven to be capable of separating phases and simulate a droplet equilibrium. Cahn numbers $Ch_L \geq 1$ and $Ch_r \leq 0.1$ are recommended for a properly resolved solution. With no convective term in the CH equation, there is no mass loss, or shift of mass. Several fluid bodies may therefore be simulated without risk. The lower limit h for separation of fluid bodies of the same type is $h \geq 25\epsilon$.

6.2   Falling Droplet

If the Cahn–Hilliard and Navier–Stokes equations are coupled for solving two-phase flow, the following mesh guidelines are recommended; $Ch_L \geq 2$, and $Ch_r \leq 0.1$. The reason why the guideline for Ch_L is different from above, is due to unequal definitions in the two solvers. The condition $Ch_r \leq 0.01$, to restrict local mass loss in the droplet, have not been tested due to severe global mass loss. The two different Cahn numbers used in this thesis are both directly proportional to the interface parameter ϵ. Ideally Ch_L should be large and Ch_r small. A practical approach to simulation is to define a droplet radius, use Ch_r to calculate the interface parameter, then use Ch_L to obtain the mesh refinement needed. In terms of the initial spacing between the droplet and the film, the same recommendation as above is valid. The separation h between fluid bodies should be no less than $h \geq 25\epsilon$ for the surfaces to be properly resolved upon impact.

All the mesh-guidelines presented in this chapter are lower limits. Further increasing the numerical resolution will give better results, at the expense of computational cost. The solver used in this thesis is based on the spectral element method, and it is not known whether the guidelines presented will hold true if a finite difference or finite volume based solver is used.

In terms of the dynamical solution; the ultimate goal of this thesis was to numerically simulate the outcome of low energy droplet-film collisions. High energy coalescence of the droplet and fluid film was observed in several simulations. The solver also displayed an apparent bouncing behaviour, however the results were not conclusive. No indications of floating or low energy coalescence was observed, this is in line with most of the previous work in the field.

The solver was found to be greatly parameter dependent. Severe mass loss is occurring using some settings, and it is reason to believe that the density and viscosity ratios are the governing parameters. The definite reason however, have not been found. As of now, high density and viscosity ratios, $\sim \mathcal{O}(10^2 - 10^3)$, are recommended.

6.3 Further Work

A major problem encountered in almost all simulations was global mass loss. Further simulations and analysis will have to be performed, with particular focus on solving the issue with mass conservation. Suggested focus of further work:

Mesh Refinement Due to time restrictions, a thorough mesh refinement has not been performed. The level of mesh dependency and rate of convergence have not been investigated. Higher order polynomial expansions have not been implemented. All of the above may help uncover the underlying problem.

Parameter Study The solver is sensitive to the parameters used. A complete parameter study, continuing the work started in section 5.2.1 is recommended. Investigating other parameters, mainly the surface tension and geometry, may be the next progression.

Boundary Conditions It is recommended to look further into the potential mass loss along

boundaries. The diffusive term is especially interesting as it showed asymmetric behaviour.

LSQ Weights Changing the relative importance of the boundary conditions when implementing the Least Squares Method may be a way of conserving mass. It is however not confirmed that the boundary conditions are the main reason for the mass loss.

Experimental Results This suggestion is not related to mass loss, but rather obtaining the correct dynamics. Attempts at directly copying experimental results can be performed. Problems may arise when the length and velocity scales are to be copied.

Mesh refinement and parameter study is recommended as primary action towards solving the problem of mass loss. Some of the physical behaviour is highly encouraging, in particular the coalescence of the fluid bodies. The author believes that if the issue of mass conservation is fixed, then the solver could be a great tool in future multiphase simulations.

[This page intentionally left blank]

Appendix A

Problem Parameters

Table A.1 – *Droplet Equilibrium, section 4.1*

Parameter	Single Droplet	Two Droplets
L_x	2	4
L_y	2	2
Ne_x	8-64	100
Ne_y	8-64	50
P[1]	4	4
ϵ	0.05-0.0025	0.01
M	1	1
Pe	1	1
r_0	0.25	0.25

Table A.2 – *Falling Droplet , section 4.2*

Parameter	0	A	B	C	D	E	F
L_x	1	1	1	0.5	0.004	0.006	0.008
L_y	2	2	2	1	0.008	0.012	0.016
Ne_x	24-36	24-36	24-36	24	24	24	24
Ne_y	48-72	48-72	48-72	48	48	48	48

Continued on next page

---

[1] Equal in all directions

Table A.2 – *Continued from previous page*

Parameter	0	A	B	C	D	E	F
Ne_z	1	1	1	1	1	1	1
P	4	4	4	4	4	4	4
ϵ	0.01-0.02	0.01-0.02	0.015-0.02	0.01	0.00008	0.00012	0.00016
Re	1000	1000	55	111.5	445	817	1260
Pe	1000	1000	100	200	25000	16667	12500
Bo	100	100	10	19.4	0.54	1.2	2.2
Fr	1	1	1	1	1	1	1
g	9.8	9.8	9.8	9.8	9.8	9.8	9.8
r_0	0.25	0.25	0.25	0.12	0.001	0.0015	0.002
ρ_1/ρ_2	100	100	100	656	830	830	830
ρ_1	100	100	100	800	996.9	996.9	996.9
μ_1/μ_2	10	2	2	106	478	478	478
μ_1	10	2	2	1.983	0.89e-3	0.89e-3	0.89e-3
σ	24.5	24.5	24.5	23.3	0.072	0.072	0.072
α	$6\sqrt{2}$	$6\sqrt{2}$	$6\sqrt{2}$	$6\sqrt{2}$	$6\sqrt{2}$	$6\sqrt{2}$	$6\sqrt{2}$
yc1[2]	1.5	1.5	1.5	0.72	0.006	0.009	0.012
yc2[3]	-	0.75	0.75	0.35	0.002	0.003	0.004
Δt	0.01	0.01	0.01	0.01	0.01	0.01	0.01

Table A.3 – *Film, section 5.2.1*

Parameter	B	C	I^ρ	I^μ
ρ_1/ρ_2	100	666	666	100
μ_1/μ_2	2	106	2	106
Mesh[4]				

---

[2]Initial droplet centre
[3]Initial film height
[4]All simulations ran on a 1x2 domain using 24x48 elements and a polynomial expansion of 4

Appendix B

Sample MATLAB Cahn–Hilliard code

The evolution of a uniform field with small, random noise into clearly separated phases using the Cahn–Hilliard equations. Credit to Lee et al. (2014). **This is not the code used in the thesis.**

```
clear all;xright = 2;yright = 1;M = 200;N = 100;
x = linspace(0.5*xright/M, xright-0.5*xright/M,M);
y = linspace(0.5*yright/N, yright-0.5*yright/N,N); h = x(2)-x(1);
[xx,yy]=meshgrid(x,y);dt = 0.1;maxiter = 500;epsilon = 4*h/(2*sqrt(2)*atanh(0.9));
xp = linspace(0,(M-1)/xright,M)'; yq = linspace(0,(N-1)/yright,N)';
Leig=-((xp.^2)*ones(1,N) + ones(M,1)*(yq'.^2))*pi*pi;
CHeig = ones(M,N)- 2*dt*Leig + dt*epsilon^2*Leig.^2;
U = 0.001*(rand(M,N)-0.5); hat_U = dct2(real(U));
for it = 1:maxiter if rem(it,10)==0
subplot(2,1,1); surf(xx',yy',real(U))
shading interp; axis([0 xright 0 yright -1 1])
subplot(2,1,2); contourf(xx',yy',real(U), [-0.9 -0.45 0 0.35 0.9])
axis image, axis([0 xright 0 yright]); getframe(gcf)
end
fU = U.^3-3*U; hat_rhs = hat_U + dt*Leig.*dct2(real(fU));
hat_U = hat_rhs./CHeig; U = idct2(hat_U);
end
```

Appendix C

Quadrature Integration

There are several ways to approximate the value of a definite integral. An intuitive approach is Trapezoidal Rule (C.1) where the area under a function is the average value of the function at two points, multiplied with the distance between the points:

$$\int_a^b f(x)dx = (b-a)\frac{f(a)+f(b)}{2} \tag{C.1}$$

This method can be extended to more advanced integration schemes like Simpson's method. A more general way of solving an integral is quadrature integration, where the integral is the sum of weighted values at certain quadrature points:

$$\int_{-1}^1 f(x) = \sum_{q=1}^Q w_q f(x_q) \tag{C.2}$$

Gauss-Legendre-Lobatto

In the quadrature integration above (eq. C.2), the weights w_q and the points x_q where the function is evaluated are needed. This can be obtained from the Gauss-Legendre-Lobatto (GLL) rule. GLL approximates the weights and integration points based on the Legendre polynomials, eq.C.3.

$$L_n(x) = \frac{1}{2^n n!}\frac{d^n}{dx^n}[(x^2-1)^n] \tag{C.3}$$

where n is an integer. Eq.C.4 show how to calculate the weights.

$$w_q = \frac{2}{n(n-1)[L_{n-1}(x_q)]^2} \tag{C.4}$$

The quadrature points x_q are the roots of the polynomial $L'_{n-1}(x)$. Using the GLL rule, the function values are evaluated on non-uniform locations within each grid, with higher resolution near the edges. Figure C.1 shows the spatial discretization of a square of unit length with a polynomial expansion of n=10.
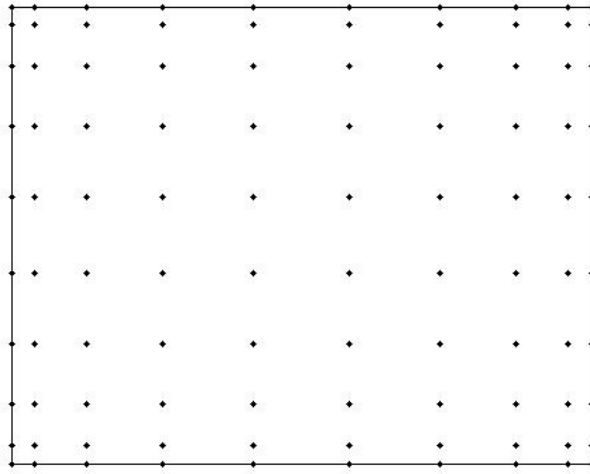
Figure C.1: 2D grid using GLL with n=10

This general method can be used in this thesis. Introducing the quadrature integration to approximate A_{ij} and F_i in eq. (2.31):

$$A_{ij} = \int_\Omega \mathscr{L}\phi_j \mathscr{L}\phi_i d\Omega \approx \sum_{q=0}^{Q} (\mathscr{L}\phi_j)|_{x_q} (\mathscr{L}\phi_i)|_{x_q} w_q \tag{C.5}$$

$$F_i = \int_\Omega g\mathscr{L}\phi_i d\Omega \approx \sum_{q=0}^{Q} g(x_q)(\mathscr{L}\phi_i)|_{x_q} w_q \tag{C.6}$$

Once the coefficients are known, insert in eq.(2.24) to obtain the full solution.

Appendix D

Physical Consistency

The solver provided to the author was simulating a droplet falling on a solid surface. The original settings are listed in table D.1.

Table D.1: Parameters in Simulation 0

Re	Pe	Bo	Fr	g	r_0	ρ_A	ρ_B	μ_A	μ_B	σ
1000	1000	100	1	-9.8	0.25	100	1	2	1	24.5

The problem with the above parameters is the physical consistency. The Froude number is defined as the ratio of inertial to gravitational forces, and in the simulations in this thesis, Fr=1 is reasonable. From the definition of the Froude number, a characteristic velocity will therefore be defined as $V = \sqrt{gL}$. With $L = 2r_0$, and the above listed surface tension, the Bond number should be 10, not 100. The Reynolds number should be ≈ 55, not 1000.

The goal is to express the dimensionless numbers in the simulations, see eqs 2.9-2.10, by use of the Weber number:

$$We = \frac{2\rho_A r_0 V^2}{\sigma} \tag{D.1}$$

The velocity will be approximated using a gravitational velocity. The actual impact velocity will be calculated from the simulations.

$$V = \sqrt{gL} \tag{D.2}$$

where g is the gravitational acceleration and $L = 2r_0$ is the characteristic length in the simulation. This definition of the characteristic velocity will make the Bond and Weber number equal, and it is a reasonable estimate of the actual impact velocity.

The rest of the dimensionless numbers can be rewritten as follows:

$$Re = \frac{2\rho_A r_0 V}{\mu_A} = We \frac{\sigma}{V \mu_A} \tag{D.3}$$

$$Bo = \frac{\rho_A g L^2}{\sigma} = We \tag{D.4}$$

$$Fr = \frac{V}{\sqrt{gL}} = 1 \tag{D.5}$$

The Peclet number have to be prescribed in advance, values will be taken from Ding et al. (2007).

$$Pe = \frac{r_0 V}{M\phi} \tag{D.6}$$

In the definitions of the dimensionless densities and viscosities, the following ratios occur. Both ratios have to be prescribed in advance:

$$\lambda_\rho = \frac{\rho_A}{\rho_B}, \lambda_\mu = \frac{\mu_A}{\mu_B} \tag{D.7}$$

To sum up, if $We, \rho_A, \rho_B, \mu_A, \mu_B$ are specified, Re, Bo, σ as well as the global viscosity and density, can be calculated. The Weber number prescribed in the solver is only an estimate, the real value have to be calculated using the actual impact velocity.

Appendix E

List of Videos

Included in the thesis is a digital folder, *master-ET.zip*, which contains the following videos. All videos are AVI-files, and should be viewable on all commercial software.

0.avi   Dynamics of Simulation 0.

A.avi   Dynamics of Simulation A.

B.avi   Dynamics of Simulation B.

C.avi   Dynamics of Simulation C.

B-film.avi   Dynamics of the fluid film simulated using settings from simulation B.

Velo-0.avi   Simulation 0 with velocity vectors superposed.

Velo-A.avi   Simulation A with velocity vectors superposed.

Velo-B.avi   Simulation B with velocity vectors superposed.

Velo-C.avi   Simulation C with velocity vectors superposed.

Velo-B-film.avi As *B-film.avi*, with velocity vectors superposed.

Bibliography

Anderson, D., McFadden, G. B., and Wheeler, A. (1998). Diffuse-interface methods in fluid mechanics. *Annual review of fluid mechanics*, 30(1):139–165.

Bewley, T. R. (2010). Numerical renaissance: Simulation, optimization, and control. *Renaissance, San Diego, CA< http://numerical-renaissance. com*.

Brackbill, J., Kothe, D. B., and Zemach, C. (1992). A continuum method for modeling surface tension. *Journal of computational physics*, 100(2):335–354.

Cahn, J. W. and Hilliard, J. E. (1958). Free energy of a nonuniform system. i. interfacial free energy. *The Journal of chemical physics*, 28(2):258–267.

Couder, Y., Fort, E., Gautier, C.-H., and Boudaoud, A. (2005). From bouncing to floating: Noncoalescence of drops on a fluid bath. *Physical review letters*, 94(17):177801.

De Maerschalk, B. (2003). Space-time least-squares spectral element method for unsteady flows.

Ding, H., Spelt, P. D., and Shu, C. (2007). Diffuse interface model for incompressible two-phase flows with large density ratios. *Journal of Computational Physics*, 226(2):2078–2095.

Fernandino, M. and Dorao, C. (2011). The least squares spectral element method for the cahn–hilliard equation. *Applied Mathematical Modelling*, 35(2):797 – 806.

Ferziger, J. H. and Peric, M. (2012). *Computational methods for fluid dynamics*. Springer Science & Business Media.

Gilet, T. and Bush, J. W. (2012). Droplets bouncing on a wet, inclined surface. *Physics of Fluids (1994-present)*, 24(12):122103.

Jacqmin, D. (1999). Calculation of two-phase navier–stokes flows using phase-field modeling. *Journal of Computational Physics*, 155(1):96–127.

Jiang, Y., Umemura, A., and Law, C. (1992). An experimental investigation on the collision behaviour of hydrocarbon droplets. *Journal of Fluid Mechanics*, 234:171–190.

Jones, A. and Wilson, S. (1978). The film drainage problem in droplet coalescence. *Journal of Fluid Mechanics*, 87(02):263–288.

Kundu, P. and Cohen, I. (2008). Fluid mechanics 4 th ed.

Lee, D., Huh, J.-Y., Jeong, D., Shin, J., Yun, A., and Kim, J. (2014). Physical, mathematical, and numerical derivations of the cahn–hilliard equation. *Computational Materials Science*, 81:216–225.

MacKay, G. and Mason, S. (1963). The gravity approach and coalescence of fluid drops at liquid interfaces. *The Canadian Journal of Chemical Engineering*, 41(5):203–212.

Nobari, M., Jan, Y.-J., and Tryggvason, G. (1996). Head-on collision of drops—a numerical investigation. *Physics of Fluids (1994-present)*, 8(1):29–42.

NTNU (2016). About vilje. https://www.hpc.ntnu.no/display/hpc/About+Vilje.

Orme, M. (1997). Experiments on droplet collisions, bounce, coalescence and disruption. *Progress in Energy and Combustion Science*, 23(1):65–79.

Pan, K.-L. and Law, C. K. (2007). Dynamics of droplet–film collision. *Journal of fluid mechanics*, 587:1–22.

Pan, Y. and Suga, K. (2005). Numerical simulation of binary liquid droplet collision. *Physics of Fluids (1994-present)*, 17(8):082105.

Proot, M. M. and Gerritsma, M. I. (2002). A least-squares spectral element formulation for the stokes problem. *Journal of Scientific Computing*, 17(1-4):285–296.

Qian, J. and Law, C. (1997). Regimes of coalescence and separation in droplet collision. *Journal of Fluid Mechanics*, 331:59–80.

Rayleigh, L. (1892). Xx. on the theory of surface forces.—ii. compressible fluids. *The London, Edinburgh, and Dublin Philosophical Magazine and Journal of Science*, 33(201):209–220.

Rein, M. (1993). Phenomena of liquid drop impact on solid and liquid surfaces. *Fluid Dynamics Research*, 12(2):61.

Scardovelli, R. and Zaleski, S. (1999). Direct numerical simulation of free-surface and interfacial flow. *Annual review of fluid mechanics*, 31(1):567–603.

Shewchuk, J. R. (1994). An introduction to the conjugate gradient method without the agonizing pain.

Tanguy, S. and Berlemont, A. (2005). Application of a level set method for simulation of droplet collisions. *International journal of multiphase flow*, 31(9):1015–1035.

Thermal Two Phase Flow Laboratory, N. (2013). Gas liquid separation: Bouncing droplet. https://www.youtube.com/watch?v=vhMXxd7ICOw.

Tryggvason, G., Bunner, B., Esmaeeli, A., Juric, D., Al-Rawahi, N., Tauber, W., Han, J., Nas, S., and Jan, Y.-J. (2001). A front-tracking method for the computations of multiphase flow. *Journal of Computational Physics*, 169(2):708–759.

van der Waals (1893). Translation of jd van der waals'"the thermodynamik theory of capillarity under the hypothesis of a continuous variation of density". *Journal of Statistical Physics*, 20(2):197–200.

Vander Wal, R. L., Berger, G. M., and Mozes, S. D. (2006). Droplets splashing upon films of the same fluid of various depths. *Experiments in fluids*, 40(1):33–52.

Xiu, D. (2010). Numerical methods for stochastic computations: a spectral method approach.

Yue, P., Zhou, C., and Feng, J. J. (2007). Spontaneous shrinkage of drops and mass conservation in phase-field simulations. *Journal of Computational Physics*, 223(1):1–9.

Zhang, F., Li, E., and Thoroddsen, S. T. (2009). Satellite formation during coalescence of unequal size drops. *Physical review letters*, 102(10):104502.

Zhao, H., Brunsvold, A., and Munkejord, S. T. (2011a). Investigation of droplets impinging on a deep pool: transition from coalescence to jetting. *Experiments in fluids*, 50(3):621–635.

Zhao, H., Brunsvold, A., and Munkejord, S. T. (2011b). Transition between coalescence and bouncing of droplets on a deep liquid pool. *International Journal of Multiphase Flow*, 37(9):1109–1119.

Zienkiewicz, O. C., Taylor, R. L., Zienkiewicz, O. C., and Taylor, R. L. (1977). *The finite element method*, volume 3. McGraw-hill London.